LA-10513-PR
Progress Report

...ratory is operated by the University of California for the United States Department of Ener... Contract W-7405-ENG-36

...plied Nuclear Scien...e Research ...nd Development Prog...ess Report

June 1, 1984 - May 31, 1985

Los Alamos
Los Alamos National Laboratory
Los Alamos, New Mexico 87545

The four most recent reports in this series, unclassified, are LA-9647-PR, LA-9841-PR, LA-10069-PR, and LA-10288-PR.

This work was performed under the auspices of the US Department of Energy's Division of Reactor Research and Technology, Office of Basic Energy Sciences, and Office of Fusion Energy.

LA-10513-PR
Progress Report

UC-34C
Issued: September 1985

Applied Nuclear Science Research and Development Progress Report

June 1, 1984—May 31, 1985

Compiled by
E. D. Arthur
A. D. Mutschlecner

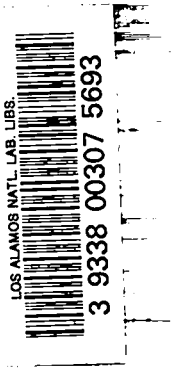

Los Alamos National Laboratory
Los Alamos, New Mexico 87545

CONTENTS

APPLIED NUCLEAR SCIENCE RESEARCH AND DEVELOPMENT
PROGRESS REPORT

June 1, 1984-May 31, 1985

Compiled by

E. D. Arthur and A. D. Mutschlecner

ABSTRACT

This progress report describes the activities of the Los Alamos Applied Nuclear Science Group for June 1, 1984, through May 31, 1985. The topical content is summarized in the Contents.

I. THEORY AND EVALUATION OF NUCLEAR CROSS SECTIONS

A. Neutron Spectra for the t + ^{6}Li Reaction [G. Hale, D. George, and P. Lisowski (P-3)]

The interaction of tritons with lithium in the blanket of a fusion reactor could have an important effect on the total neutron spectrum. We have continued our interpretation of recent measurements[1] of t + ^{6}Li neutron spectra, using the 3-body resonance model implemented in the code SPECTRA.

The calculations are illustrated in the spectra shown in Figs. 1 and 2. They contain "direct" contributions from the first five levels in ^{8}Be, in addition to a broad, underlying "exchange" contribution from the ground state of ^{5}He. The amplitudes of these contributions were adjusted to describe the zero-degree spectrum at E_t = 1.64 MeV shown in Fig. 1, and to give also a good representation of low-energy ^{6}Li(^{3}He,p) spectra.[2] These amplitudes were found to give a surprisingly reasonable description of the ^{6}Li(t,n) spectra over the range of energies ($1.6 \leq E_t \leq 4.5$ MeV) and angles ($0° \leq \theta_n \leq 150°$) measured at Los Alamos, as illustrated in Fig. 2.

At incident triton energies above 2 MeV, there is evidence (Fig. 2c) for structure at low neutron emission energies coming from p + ^{7}Li resonances in ^{8}Be at excitation energies above 17 MeV. We have modified the code to accommodate both the α-α and p-^{7}Li channels in ^{8}Be, and have made some progress accounting for the observed low-energy structure.

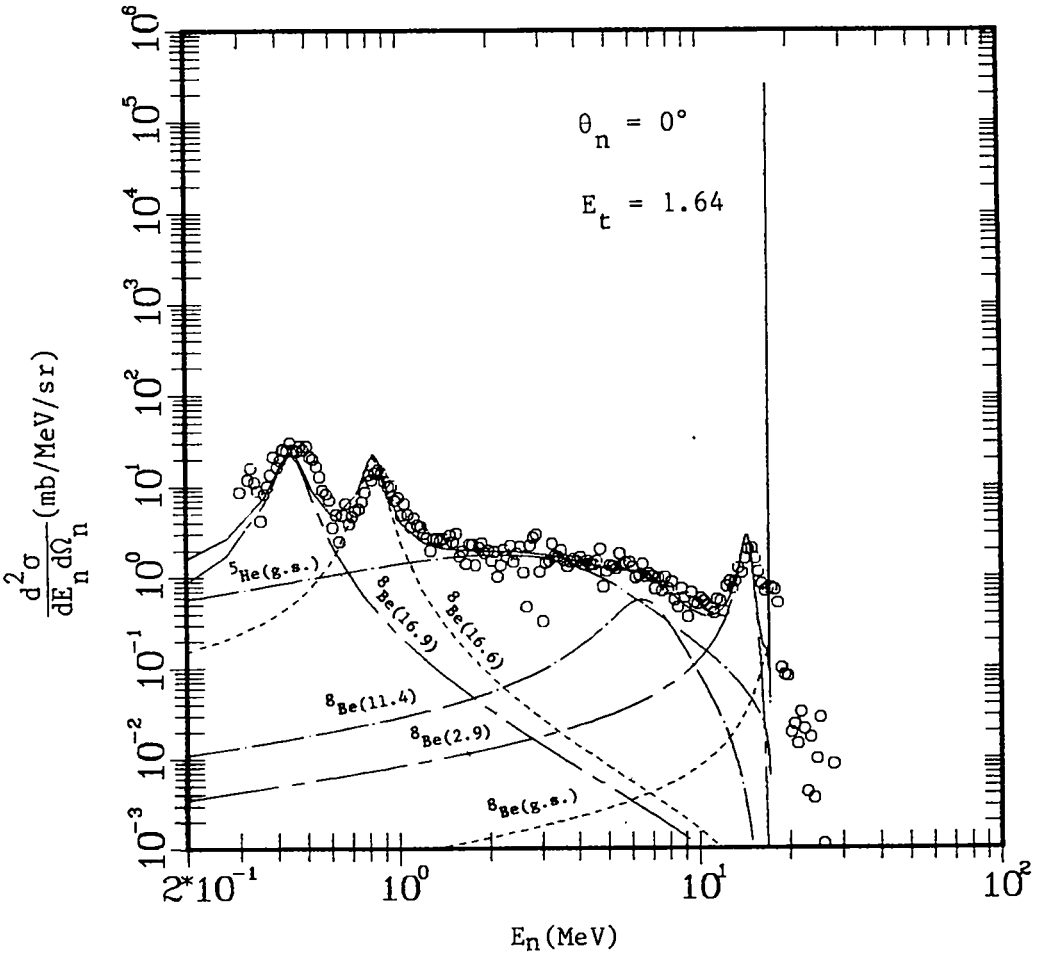

Fig. 1. Calculated and measured ^{6}Li(t,n) laboratory spectra at θ_n = 0° for E_t = 1.64 MeV, showing the various components of the calculation (solid curve).

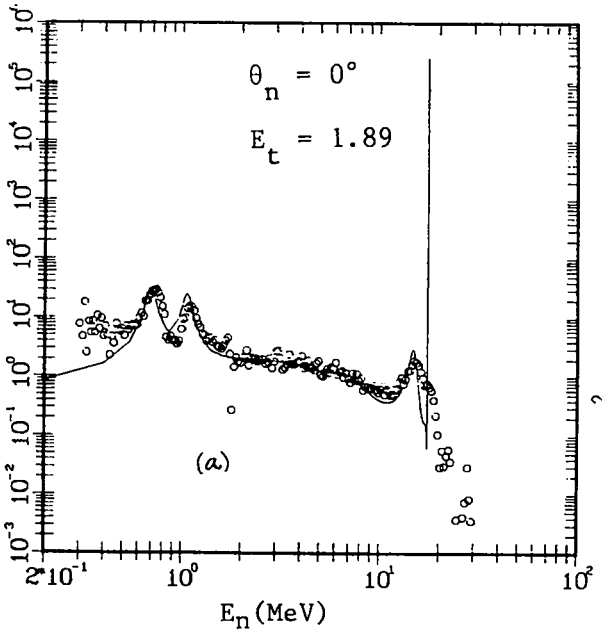

Fig. 2a.

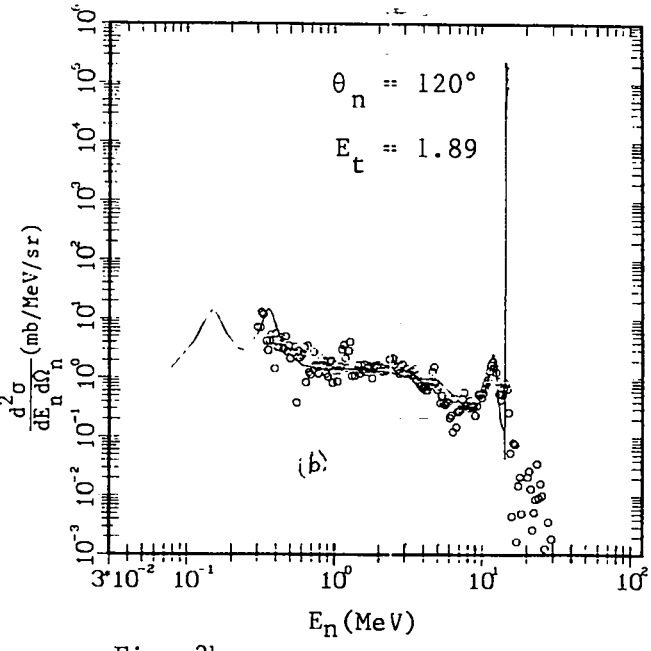

Fig. 2b.

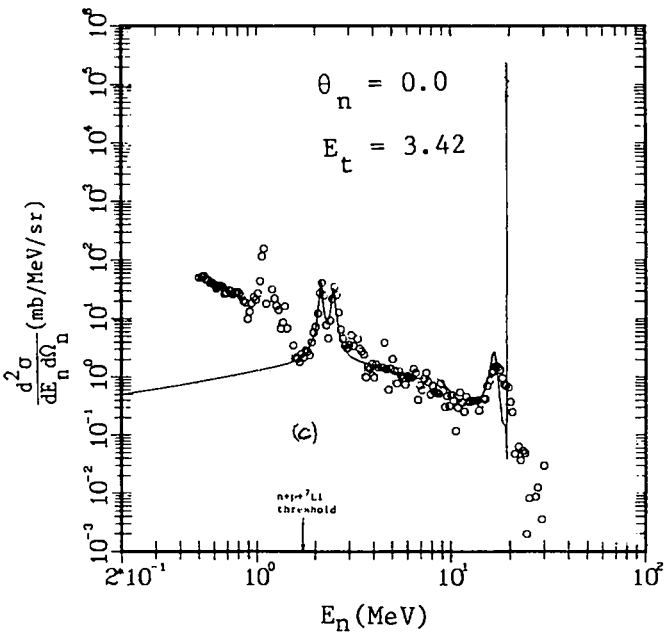

Fig. 2c.

Fig. 2. Calculated and measured $^{6}Li(n,t)$ laboratory spectra at (a) $\theta_n = 0°$ and (b) 120° for $E_t = 1.89$ MeV, and at (c) $\theta_n = 0°$ for $E_t = 3.42$ MeV. The parameters of the calculation are the same as those used in Fig. 1.

B. Neutron-Induced Reactions on ^{11}B (P. G. Young)

The present ENDF/B-V evaluation for n + ^{11}B reactions is based on a 1966 U.K. Atomic Energy Agency analysis and does not incorporate any modern experimental or theoretical results. As pointed out in a recent review,[3] discrepancies of up to 40% exist between new measurements and the evaluated total and elastic cross sections. Even larger inconsistencies occur for elastic angular distributions. Additionally, the ENDF/B-V evaluation does not include gamma-ray production data.

A new evaluation of n + ^{11}B data for neutron energies up to 20 MeV is in progress at Los Alamos. To complement the available experimental data and to facilitate interpolation and extrapolation in the evaluation, an optical model/reaction theory analysis of the experimental data is being performed.

Figure 3 compares an early scoping calculation (pg. 4 of Ref. 4) of the gamma-ray emission spectrum from 14.5-MeV neutrons on ^{11}B with preliminary experimental data from a recent measurement by Group P-3 at Los Alamos.* This measurement includes data for neutron energies between 2-42 MeV at five angles for gamma-ray energies between 1.6 and 19 MeV, and it provides one of the major new sources of data for the evaluation.

The neutron transmission coefficients used in the calculation for Fig. 3 were obtained from an optical model analysis of n + ^{14}N data, as described in Ref. 4, using the GNASH Hauser-Feshbach, statistical theory code.[5] The final analysis will be further optimized for consistency with the P-3 gamma-ray experiment, as well as with modern measurements of neutron total cross sections and scattering angular distributions.

---

*This measurement was provided by G. Auchampaugh and S. Wender, Group P-3, of the Los Alamos National Laboratory in 1984.

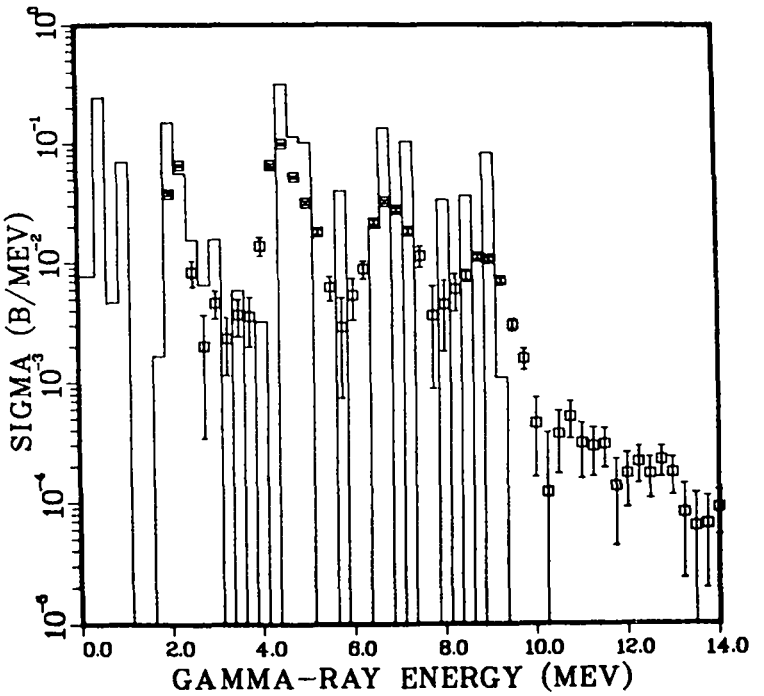

Fig. 3. Comparison of a calculated gamma-ray emission spectrum from 14.5 MeV neutrons on ^{11}B with preliminary experimental data (squares) from Los Alamos. Note that the calculated histogram has not been broadened for experimental resolution. The measured data have been averaged over the five angles of the measurement.

C. Nuclear Data for Natural Silver (P. G. Young)

The existing ENDF/B-V data base includes evaluations for the silver isotopes ^{107}Ag and ^{109}Ag, but does not provide either gamma-ray production information or data of any sort for the natural element. Because these data are required in certain applications, an interim evaluation for n + ^{NAT}Ag has been assembled from the neutron data in ENDF/B-V for ^{107}Ag and ^{109}Ag, and the 1973 gamma-ray production evaluation by Young.[6]

ENDF files 2-5 were constructed mainly using R. MacFarlane's NJOY/MIXER code.* All the discrete inelastic level reactions from the ^{107}Ag and ^{109}Ag evaluations are retained in the natural file. The only change made to the neutron data was to add a semi-direct radiative capture component to the MF=3, MT=102 cross section for E_n > 3.5 MeV. This modification appears as an enhancement above E_n = 8 MeV in the radiative capture cross section, as illustrated in Fig. 4. The maximum value of the cross section in this region is ~ 1 mb near 14 MeV and results in the emission of high energy gamma rays (described below). The elastic neutron cross section was appropriately reduced to absorb this change while keeping the total cross section unchanged.

*This information was provided by R. E. MacFarlane, Los Alamos National Laboratory in October 1984.

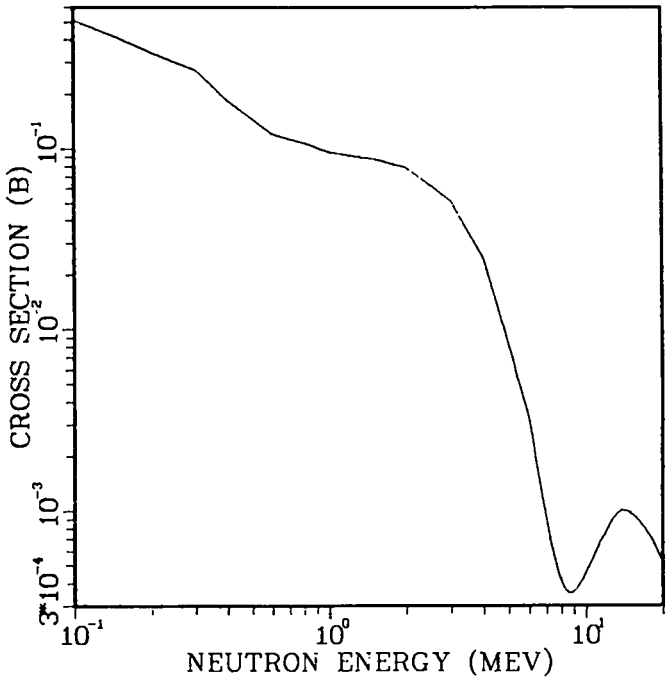

Fig. 4. Evaluated (n,γ) cross section for natural Ag from 0.1-20 MeV.

The gamma-ray production data included in the natural evaluation were mainly taken from a 1973 evaluation.[6] The gamma-ray spectrum at thermal energies is based on a measurement by Orphan et al.,[7] which was smoothly joined to a spectrum at 0.0888 MeV inferred from the spectral measurement of Dickens* between E_n = 0.8 and 20 MeV. Because Dickens' data had a low-energy cutoff of approximately E_γ = 0.5 MeV, the empirical formulas of Howerton[8] were used to extrapolate the spectra to zero gamma-ray energy. Unlike the earlier gamma-ray data evaluation,[6] the present file was split at E_n = 0.0888 MeV (the inelastic threshold) into a low-energy component (MT=102; MF=12, 14, 15) and a high-energy component (MT=3; MF=13, 14, 15).

A comparison of the evaluation (solid curve) with Dickens' data at E_n ~ 2.24 MeV is given in Fig. 5. Although the extrapolation to E_γ = 0 is a minor extension of the spectrum, it does introduce an appreciable uncertainty in the total production cross section due to the peaking of the spectrum at low gamma energies. Note in Fig. 5 that the component of the spectrum at E_γ > 2.24 MeV is due to radiative capture.

---

*This measurement was supplied by J. K. Dickens, Oak Ridge National Laboratory in 1973.

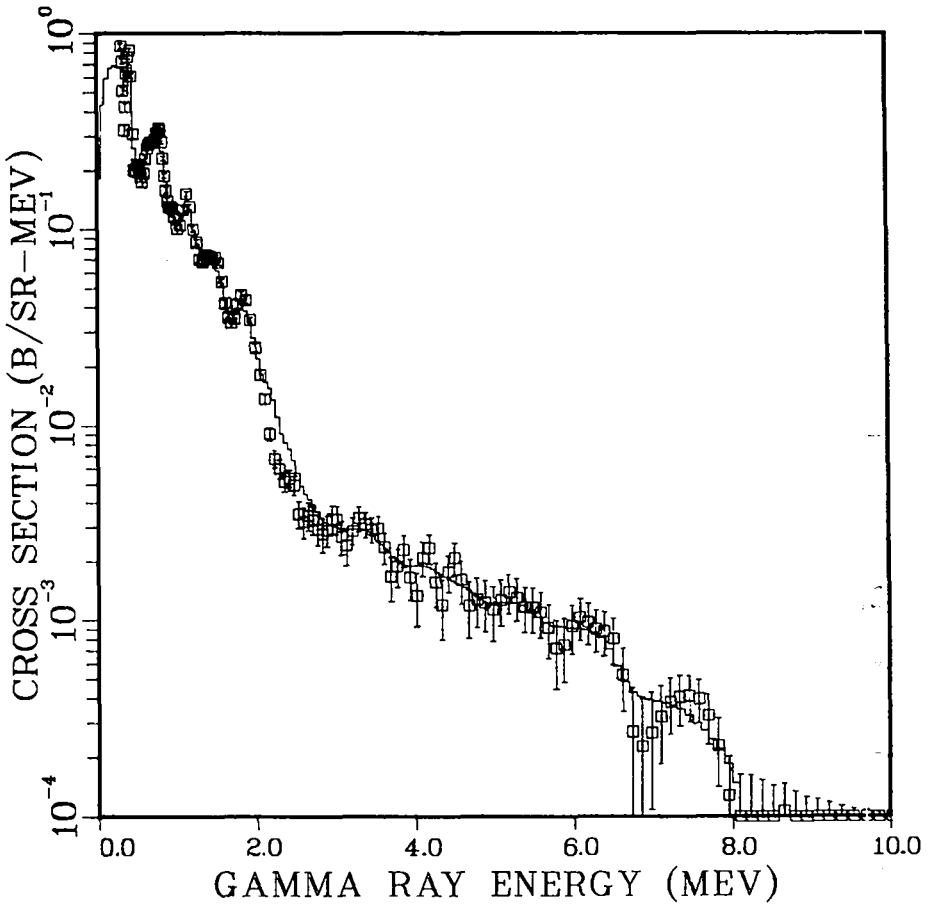

Fig. 5. Comparison of the evaluated gamma-ray emission spectrum for 2.24-MeV neutron bombardment of natural Ag with the experimental data of Dickens.*

The earlier gamma-ray production evaluation did not include the effects of semi-direct radiative capture. While such effects are not large, they do result in high-energy gamma rays that might be important in some applications. To correct this deficiency, a semi-empirical model developed by E. Arthur** was used to obtain the energy dependence of the semi-direct capture cross section for E_n = 5-20 MeV (normalized to ~ 1 mb at E_n = 14 MeV) and to calculate the corresponding gamma-ray spectrum. These effects were combined into the previous gamma-ray data evaluation. Figure 6 illustrates the effect of semi-direct capture on the gamma-ray spectrum at E_n = 13 MeV, by the pronounced peak near E_γ = 15 MeV.

It should be emphasized that the present ^{NAT}Ag evaluation is the result of a very limited effort that mainly combines three older evaluations without any significant effort to update them. This evaluation should therefore be regarded as interim until a more thorough analysis can be completed.

* This was provided by J. K. Dickens, Oak Ridge National Laboratory in 1973.

**This model was developed by E. D. Arthur, Group T-2 of the Los Alamos National Laboratory in 1973.

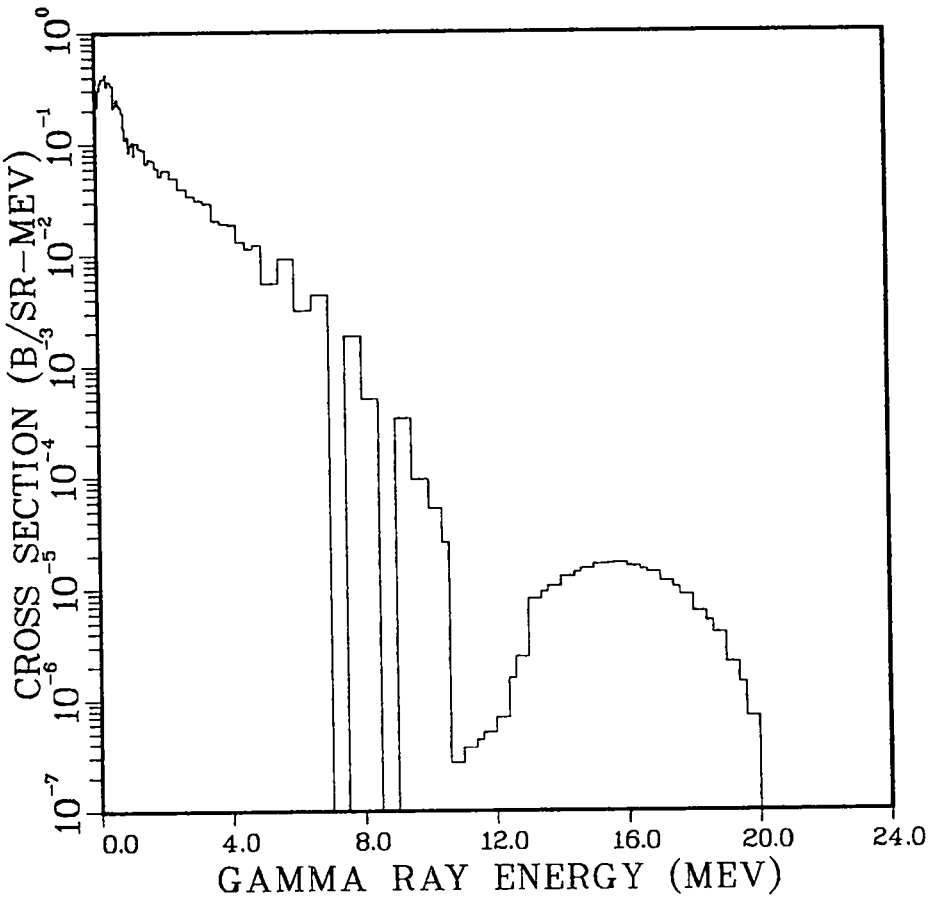

Fig. 6. Evaluated gamma-ray emission spectrum from 13-MeV neutron interactions on ^{NAT}Ag.

D. Conversion of the GNASH Reaction Theory Code to CRAY Computers [P. G. Young and K. Witte (C-3)]

The conversion of the GNASH Hauser-Feshbach statistical, preequilibrium code[5] from CDC-7600 to CRAY computers has been completed. In the course of the conversion, a number of improvements were made that greatly increased the flexibility of the code for different types of problems and improved the efficiency (speed) of all calculations.

All the major variable dimensions were consolidated into a single PARAMETER statement, which permits quick reallocation of storage space to optimize for particular problems. In addition, all dimensions can be readily increased to utilize the much greater memory capacity of the CRAY relative to the 7600 computers. Table I compares the dimensions of one memory configuration for the CRAY version with the previous 7600 version. (This configuration by no means exhausts the capacity of the CRAY X-MP computers.)

TABLE I

GNASH DIMENSIONS

	CDC 7600	CRAY X-MP
No. Compound Nuclei (CN)	8	10
No. Reaction Channels/CN	4	6
No. Energy Bins	100	160
No. Discrete Levels/Nuc.	35	300
No. Discrete Gammas/Nuc.	70	900

The efficiency improvements incorporated into the CRAY version of GNASH improved its speed by a factor of 6 over the 7600 version. Extensive calculations of neutron-induced reactions on ^{93}Nb and ^{239}Pu, based on analyses performed in the past,[9,10] were carried out to test the new versions. In all cases, results identical to those from the 7600 version of GNASH were obtained.

E. Documentation of Revisions of ENDF/B-V [B. A. Magurno (Brookhaven National Laboratory) and P. G. Young]

A series of summary documents has been compiled and edited into a complete report describing all modifications made to the ENDF/B-V evaluated nuclear data base during Revisions 1 and 2.[11]

F. Calculation of Proton-Induced Reactions on Copper at E ≦ 50 MeV (E. D. Arthur)

We used the GNASH Hauser-Feshbach preequilibrium nuclear model code[5] to calculate cross sections for proton reactions on ^{63}Cu and ^{65}Cu. The highest incident energy included was 50 MeV, while the lower bound coincided with the threshold for (p,n) reactions (~ 4.5 MeV for ^{63}Cu and 2.25 MeV for ^{65}Cu). The primary purpose of the calculations was provision of microscopic nuclear data required for thick-target neutron yields applicable to accelerator design. These thick target results are described later in this progress report.

The input parameters used were derived principally from our previous calculational studies[12,13] of neutron-induced reactions on structural materials at incident energies up to 50 MeV. Table II summarizes the neutron and proton optical parameters employed here. Parameters for alpha-particle emission are not shown, but were based on the modified Lemos[14] parameters, as described in Ref. 12. We determined gamma-ray strength functions by adjustment of calculated capture results to agree with $^{63,65}Cu(n,\gamma)$ experimental data. Three gamma-ray multipolarities were included--E1, M1, E2. A giant dipole resonance form[15] was employed for the E1 gamma-ray strength function, while the Weisskopf[16] estimate (suitably normalized) was used for M1 and E2 radiation. The results obtained here generally agreed with previous gamma-ray strength functions determined for iron and nickel isotopes,[12] as well as our recent results obtained for titanium and vanadium isotopes.[17]

Because the determination of total neutron emission was the primary goal of this effort, we made several preliminary calculations to optimize the reaction sequence to be included in the problem. These steps were necessary even

TABLE II

NEUTRON AND PROTON OPTICAL PARAMETERS[a] USED FOR p + Cu CALCULATIONS

Neutrons	r	a
$V = 47.76 - 0.364E - 0.0003E^2$	1.287	0.56
$W_{VOL} = -0.072 + 0.148E$	1.345	0.47
$V_{SO} = 6.2$	1.12	0.47
$W_{SD} = 8.11 + 0.0805E$	1.345	0.47
Above 6 MeV		
$W_{SD} = 8.6 - 0.25E$		

Protons	r	a
$V = 58.35 - 0.55E$	1.25	0.65
$V_{SO} = 7.5$	1.25	0.47
$W_{SD} = 13.5 - 0.15E$	1.25	0.47
$r_c = 1.25$		

[a]All well depths in MeV; geometrical parameters in fermis.

though the new CRAY version of GNASH (described elsewhere in this progress report) offers increased flexibility for including more complex decay schemes. The initial calculations allowed us to discard minor reaction paths that require significant computational time while contributing little to the overall neutron yield. We were also able to avoid overlooking major neutron-producing paths. Our first calculational attempt concentrated principally on (p,xn) reaction paths in a manner similar to chains used in neutron-induced reactions on structural materials. However, binding energy differences between neutrons and protons in the copper isotopes and their residual by-products caused significant underprediction of the total neutron yield when this approach was taken. Instead (p,xnyp) reaction paths [(p,pn), (p,p2n), (p,2pn), for example] contributed principally to the neutron emission process and had to be included explicitly. Figure 7 illustrates the complexity of the reaction sequence finally used for our p + ^{63}Cu calculation. The availability of the new CRAY version of GNASH simplified the effort required for higher energy calculations in that all major reaction chains could be included in one calculational pass and the computational time required was at least ten times less than for the previous CDC 7600 version. The CRAY central processor time required for the 50 MeV calculation was approximately two minutes.

Final calculations were made for p + ^{63}Cu and p + ^{65}Cu reactions at incident energy intervals of 5 MeV extending up to E_p = 50 MeV. Because the GNASH code produces only angle-integrated emission spectra, we used the Kalbach-Mann[18] systematics, along with our calculated preequilibrium fractions to produce emitted neutron spectra covering the angular range from 0° to 180° in 15° intervals. Examples of neutron spectra produced for 50-MeV protons on ^{65}Cu at angles of 0°, 15°, and 45° appear in Fig. 8.

Although determination of neutron-emission spectra was the primary goal of these calculations, we also computed cross sections for (p,xn) and (p,xnyp) excitation functions that can be compared with experimental data. Figures 9-12 show selected examples of such results. Generally, there is good agreement although higher energy (p,n) and (p,pn) results are underpredicted. This could indicate the need to include a greater preequilibrium contribution in the calculations. However, the preequilibrium fraction required may be unphysically large, especially in the case of the (p,pn and p,np) reactions where a 50-75 millibarn discrepancy exists between the calculation and experiment. Another contributing factor in the case of the theoretical (p,pn and p,np) underprediction may be too much competition from (p,p2n) reactions [actually (p,pnn),

(p,npn) or (p,nnp) results]. This would indicate overprediction of low-energy neutron emission, which may be linked to the low-energy behavior of the neutron transmission coefficients used or the size of the integration bin (1 MeV) used in the calculation. Further efforts are under way to identify the cause of this discrepancy.

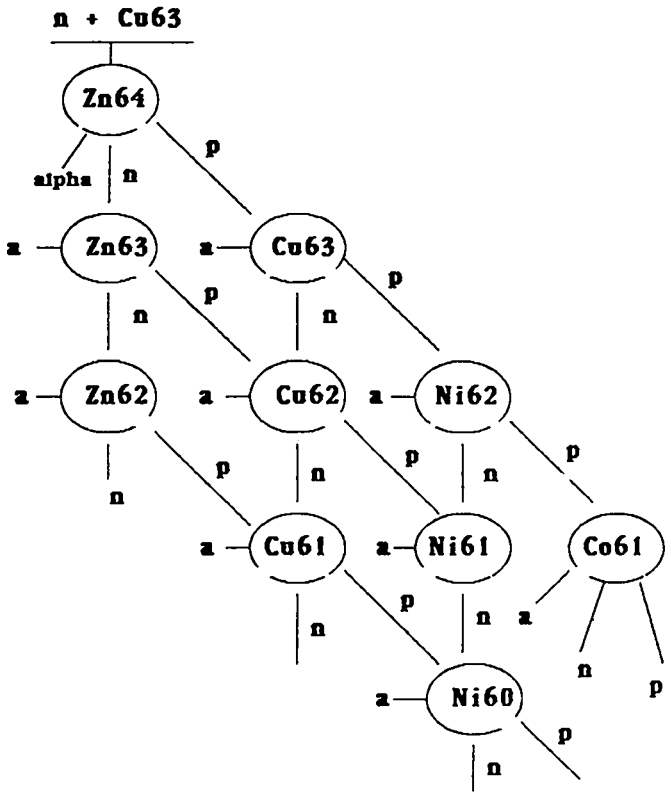

Fig. 7. Reaction schematic used in the calculation of 50-MeV proton interactions with ^{63}Cu.

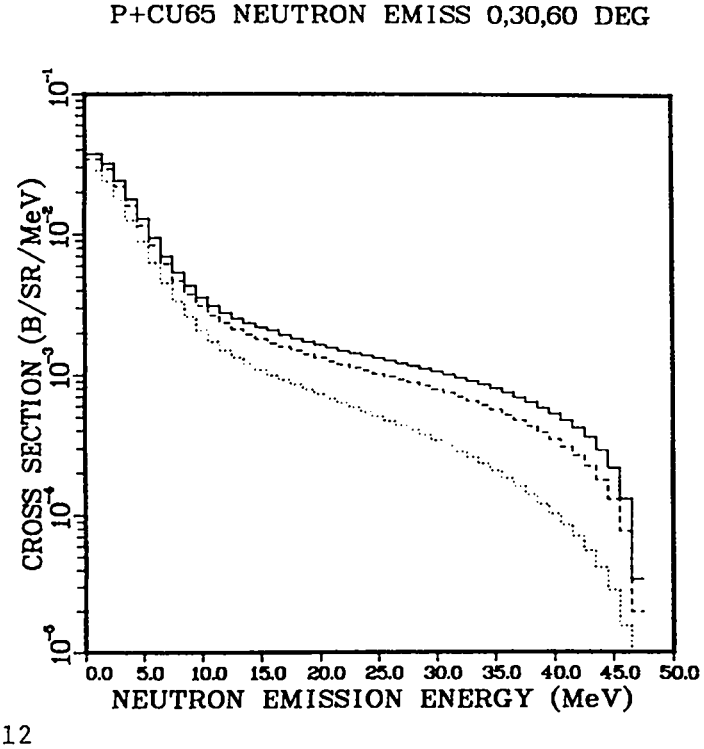

Fig. 8. Examples of neutron emission spectra for angles of 0° (solid), 15° (dashed) and 45° (dotted) curves, as determined from GNASH calculated results used in conjunction with the Kalbach-Mann systematics.

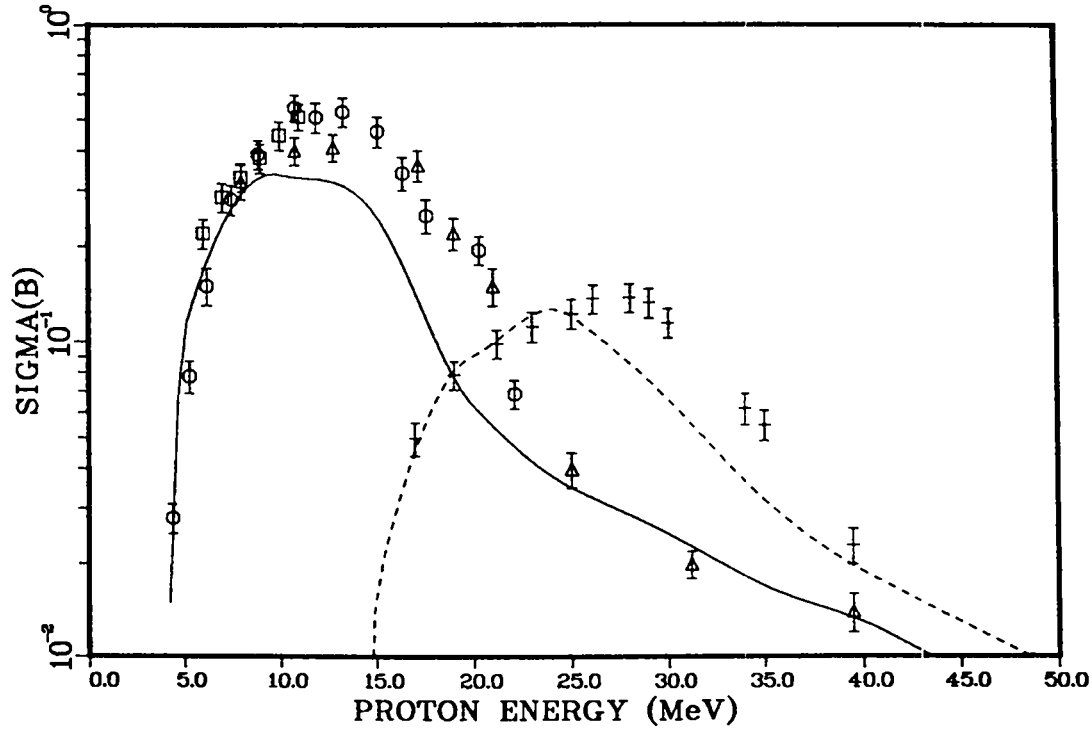

Fig. 9. Excitation functions for proton induced reactions on ^{63}Cu. Triangles circles, squares are (p,n) data[19,20]. Horizontal lines (with error bars) represent (p,2n) data.[19]

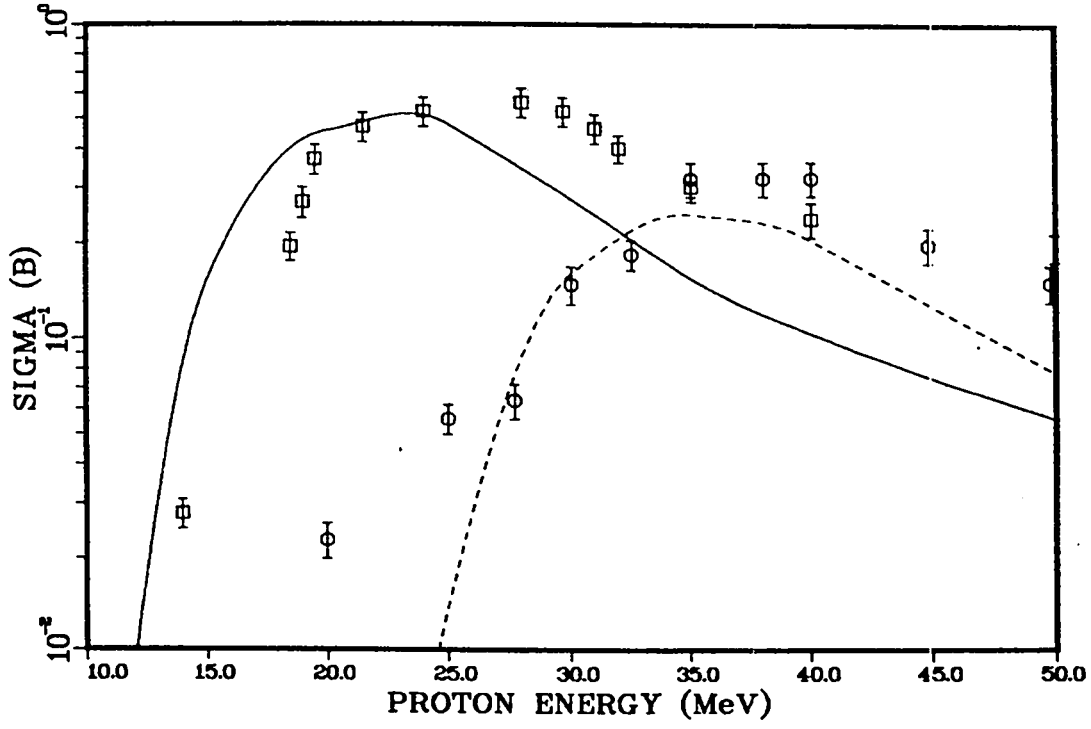

Fig. 10. More excitation functions for proton induced reactions on ^{63}Cu. Squares are (p,pn) data[19,20] while circles represent (p,p2n) experimental results.[19]

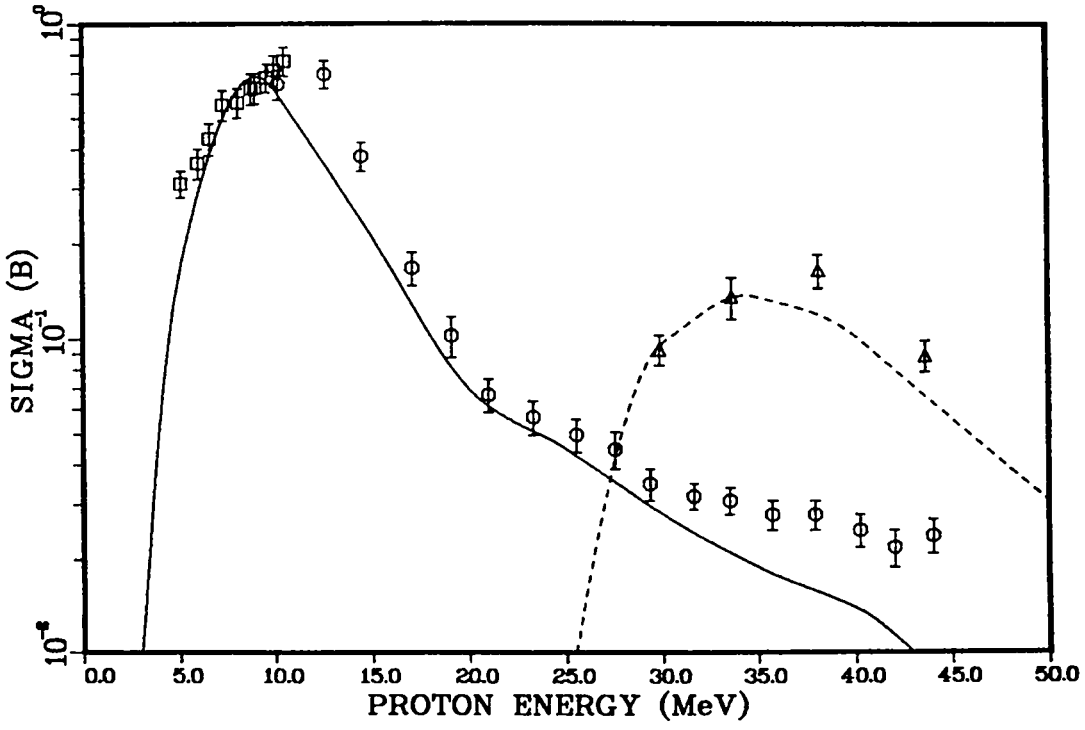

Fig. 11. Reaction data for ^{65}Cu. Squares and circles are (p,n) data[19,20] while triangles represent (p,3n) data.[20]

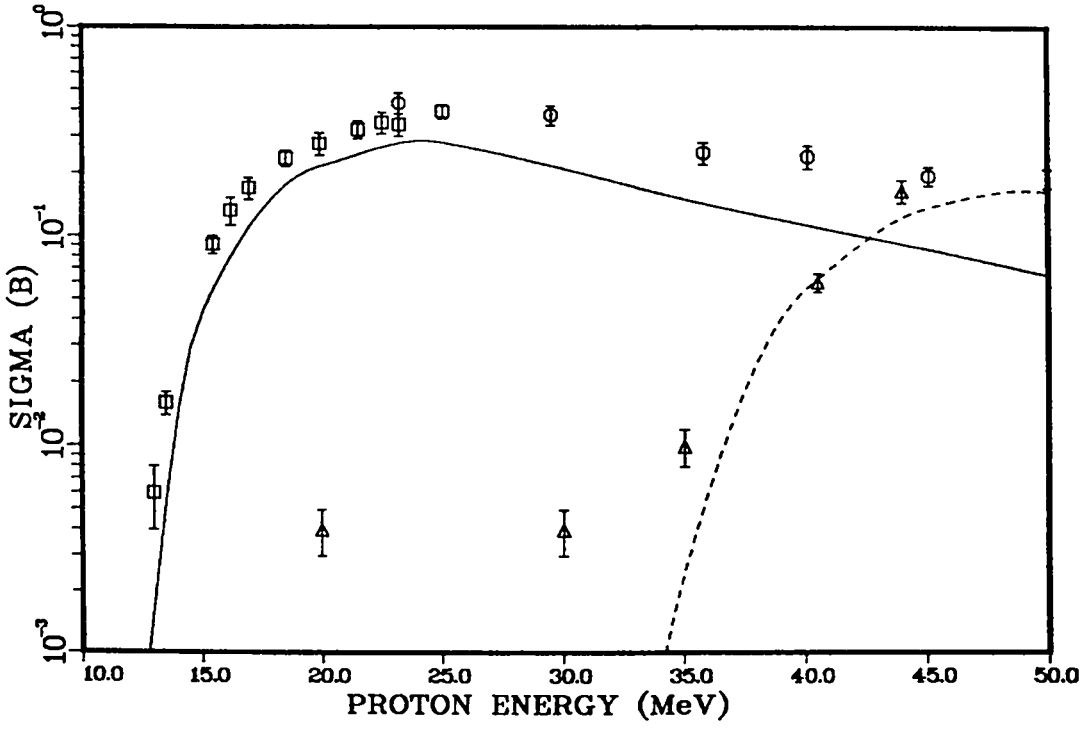

Fig. 12. Data[19,20] for (p,pn) (squares and circles) and (p,p3n) reactions (triangles) on ^{65}Cu are compared with the present calculations.

G. A Computerized Capability to Search Nuclear Structure Data Files (D. C. George and E. D. Arthur)

A program RDCD has been written to search portions of the CDRL[21] nuclear structure library and to identify and tabulate nuclear level properties of interest for nuclear model calculations or other applications. As a matter of background, the CDRL library is a computer-readable assembly (by R. J. Howerton, Lawrence Livermore National Laboratory) of particle-induced and nuclear decay data contained in the 1978 Table of Isotopes compilation.[22] The present version of RDCD is oriented towards identification of nuclear isomeric states after which nearby levels having much shorter (or instantaneous) lifetimes are displayed. The user can provide as input the desired halflife range of the isomeric states to be considered, as well as the energy spacing (in keV) over which nearby levels are to be identified.

Searches have been made in which isomeric state lifetimes were specified to be $\geq$ 10 seconds, and in which the range of energy separations of nearby levels was set equal to 0.01, 0.005, 0.002, and 0.001 MeV. Figure 13 illustrates some of the candidate nuclei identified with $\tau_{\frac{1}{2}} \geq 10$ seconds and ΔE = 0.005 MeV.

Although the RDCD code provides a useful method for making such data searches, there are some difficulties with the CDRL library that limit its usefulness. The main problem relates to the fact that the Table of Isotopes compilation upon which the library is based is current only to 1978. Thus, newer, more relevant data are missing. There are also instances where the experimental sources do not provide complete information concerning the characteristics of a level (particularly spin and/or parity) and default information (null spin and/or parity values) have been provided that can produce misleading information from RDCD. One then must refer to the original figures of Ref. 20 or the experimental works cited. Probably most serious is the frequent lack of detailed gamma-ray branching information. This situation severely limits the usefulness of such a computerized nuclear structure library in nuclear model applications. Of course, most of the difficulties result from basic data deficiencies, rather than problems with the form of the CDRL library itself.

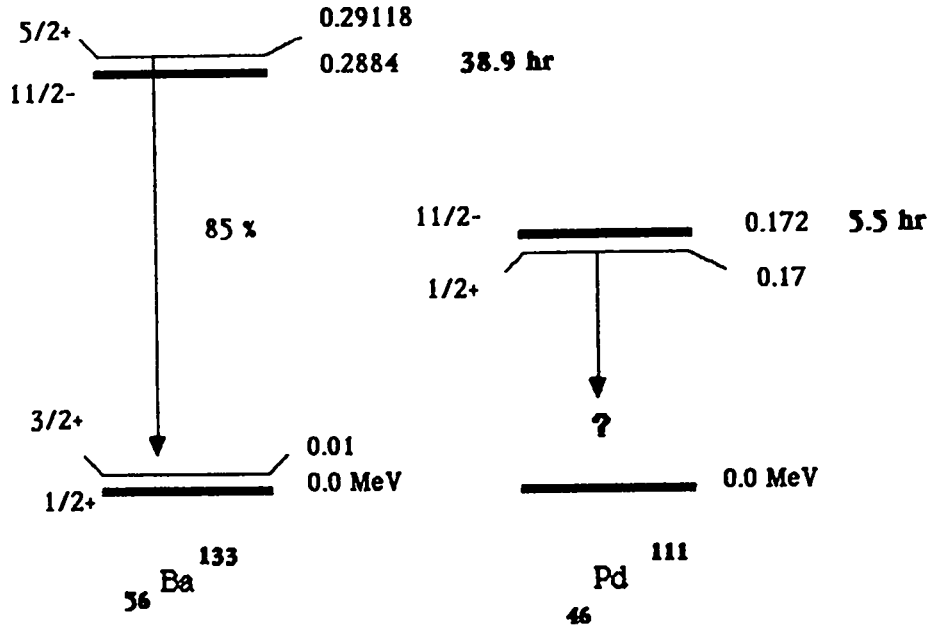

Fig. 13. Examples of nuclear level information identified with the RDCD code.

H. Microscopic Nuclear Level Density Calculations (B. Strohmaier, [T-2 Collaborator, on Leave from Institut für Radiumforschung und Kernphysik, Univ. of Vienna)]

This effort has been aimed at the study of nuclear level densities using microscopic approaches based on the moments[23] and Lanczos methods.[24] This work has been carried out in close collaboration with S. M. Grimes, Ohio University, and S. D. Bloom, Lawrence Livermore National Laboratory.

Initially, calculations using the Lanczos technique were made for ^{28}Si, which were a continuation of similar studies begun by S. D. Bloom (LLNL) and H. K. Vonach (Univ. of Vienna). Calculations were carried out in a $d_{5/2}$ $s_{1/2}$ $d_{3/2}$ $f_{7/2}$ basis, assuming a closed ^{16}O core, with certain limitations on the number of nucleons outside the $d_{5/2}$ orbital. As the basis size for this case is very large (~ 260 000 Slater determinants) and requires truncation, it was not clear whether these calculations yielded a realistic description of the level density of ^{28}Si.

In order to investigate such questions and to compare the Lanczos and moment methods, a corresponding study was begun for ^{20}Ne. This nucleus was chosen because the size of the dsdf basis is small enough so that a full (untruncated) basis calculation can be made. Thus, basis-truncation effects and possible solutions to them can be investigated. This ^{20}Ne study has been completed and a comprehensive paper based on this investigation has been submitted to Physical Review C.

Now the mass region between A = 23 and 33 has been chosen for further investigation because of the appropriateness of the relevant bases to give a realistic description of the level densities, and existence of experimental data. Retrieval of experimental level density information for ^{24}Mg from the literature has been done successfully, and first moment method calculations have been performed. Comparison of these results to the experimental data is very encouraging, but an investigation of how strongly parameter variations affect the results still seems to be required.

In addition to these calculations, efforts are underway to deal with the effects of basis truncation, as mentioned in the ^{20}Ne paper. In particular, a method of correcting the positions and widths of the pseudoeigenvectors of truncated basis calculations is being pursued. This requires finding systematics for these changes under the condition of basis truncation. Also, development and alteration of the shell model code are in progress, aiming at both inclusion of new features to the algorithm for calculating moments and exportability of the program to Europe.

I. Semi-Microscopic Calculations of Elastic, Inelastic, and Total Neutron Scattering by ^{239}Pu [D. G. Madland, Ch. Lagrange (Bruyères-le-Châtel), and M. Girod (Bruyères-le-Châtel)]

The purpose of the present work is first to investigate the capabilities of a semi-microscopic optical-model potential involving fewer adjustable parameters than phenomenological models and second to test the sensitivity of this potential to various rotational band assumptions. Our analysis of the model capabilities is performed using experimental elastic, inelastic, and total cross sections from ~ 10 keV to 15 MeV as well as neutron strength functions, and our sensitivity study is performed for the first three bands of ^{239}Pu: $1/2^+$ (0.0), $5/2^+$(286 keV), and $7/2^-$(392 keV). The two main ingredients of our calculations are the microscopic optical-model potential of Jeukenne, Lejeune, and Mahaux[25] (JLM) and nuclear densities from Hartree-Fock calculations performed using the density-dependent force D1.[26] Note that the Hartree-Fock density is calculated separately for each rotational band considered and that the coupled-channel calculations are performed for each band individually.

The present calculations differ from those previously reported[27] by the presence of an effective mass factor in front of the JLM imaginary potential. The parameters of the semi-microscopic model are mainly determined by adjustments with respect to the strength functions and total cross section over the

full energy range. The consistency of the parameterization is tested by comparisons of calculated and measured elastic and inelastic angular distributions. Our final values for the ranges of the effective interaction are t_R = 1.3 fm and t_I = 1.4 fm. The renormalization factor of the real potential is N_R = 0.935 while that of the imaginary potential is N_I = 0.46 for 10 keV $\leqq E_n \leqq$ 4 MeV, but is then rising linearly with energy to a value N_I = 0.82 at E_n = 14 MeV. The results of our calculations are summarized in Figs. 14 and 15 and Table III where they are compared with experiment and with the results obtained using the phenomenological coupled-channel potential of Ref. 28 with β_2 = 0.20 and β_4 = 0.08. The main effect of the rotational band assumption (not shown here) is on the diffraction minima of the elastic angular distributions.

More detailed calculations on the n + ^{239}Pu system are in progress. In particular, we are studying the origin of the shape sensitivity of the elastic scattering diffraction minima to the rotational band assumption (K quantum number).

TABLE III

CALCULATIONS FOR n + ^{239}Pu

E_n = 10 keV

Coupling Basis	$S_0 \times 10^4$	$S_1 \times 10^4$	R' (fm)	σ_{tot} (b)
$1/2^+,\ldots,9/2^+$ micro.	1.042	1.924	9.15	15.58
$1/2^+,\ldots,9/2^+$ phenom.	1.245	2.221	9.084	16.30
Experiment	1.3 ± .1	2.3 ± .4	9.6 ± .3	—
$5/2^+$, $7/2^+$, $9/2^+$ micro.	0.979	1.728	9.15	15.26
$7/2^-$, $9/2^-$, $11/2^-$ micro.	1.029	1.738	9.16	15.49

E_n = 3.4 MeV

Coupling Basis	σ_{el} (mb)	σ_1 (mb)	σ_2 (mb)	σ_3 (mb)	σ_4 (mb)	σ_{tot} (mb)
$1/2^+,\ldots,9/2^+$ micro.	4353	162.8	240.8	65.8	80.4	7853
$1/2^+,\ldots,9/2^+$ phenom.	4414	139.4	206.0	58.5	71.2	8010
Experiment	[4271 ± 581]		[380 ± 39]	—	—	8022 ± 100
$5/2^+$, $7/2^+$, $9/2^+$ micro.	4356	266.3	176.3	—	—	7755
$7/2^-$, $9/2^-$, $11/2^-$ micro.	4448	238.4	137.4	—	—	7776

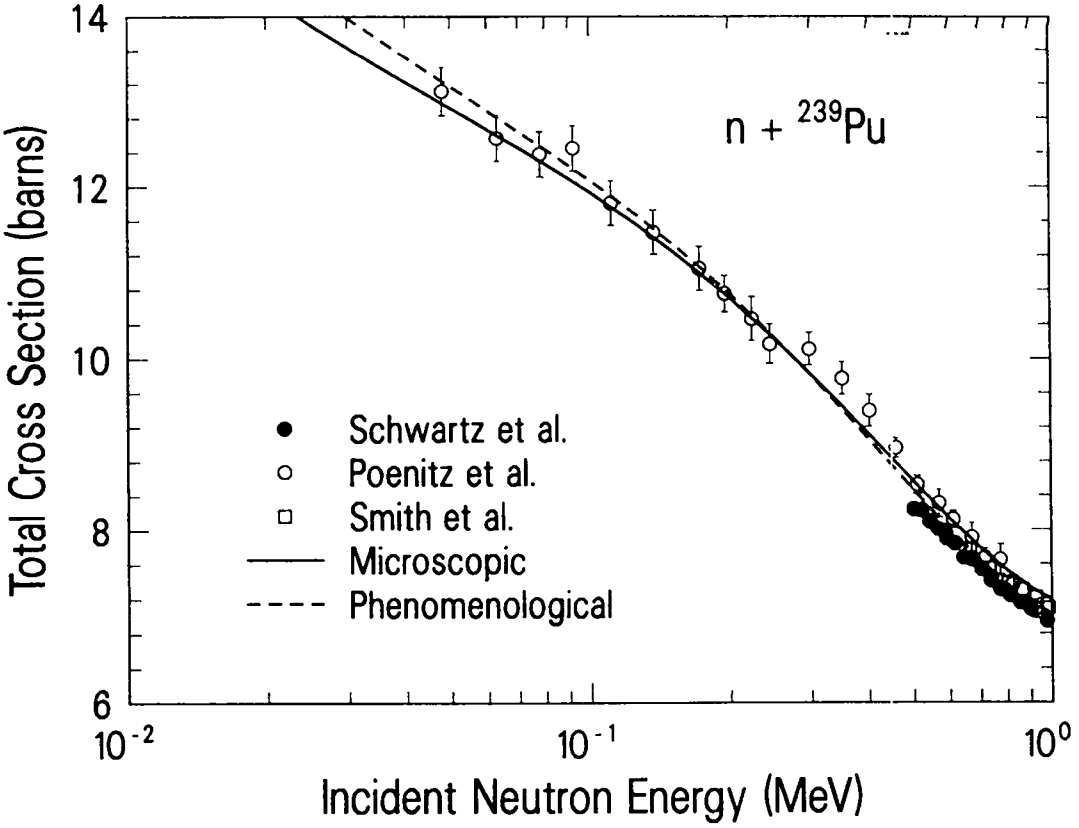

Fig. 14. Comparisons of calculated and experimental total cross sections for n + ^{239}Pu scattering over the incident neutron energy range 10 keV $\leqq E_n \leqq$ 1 MeV.

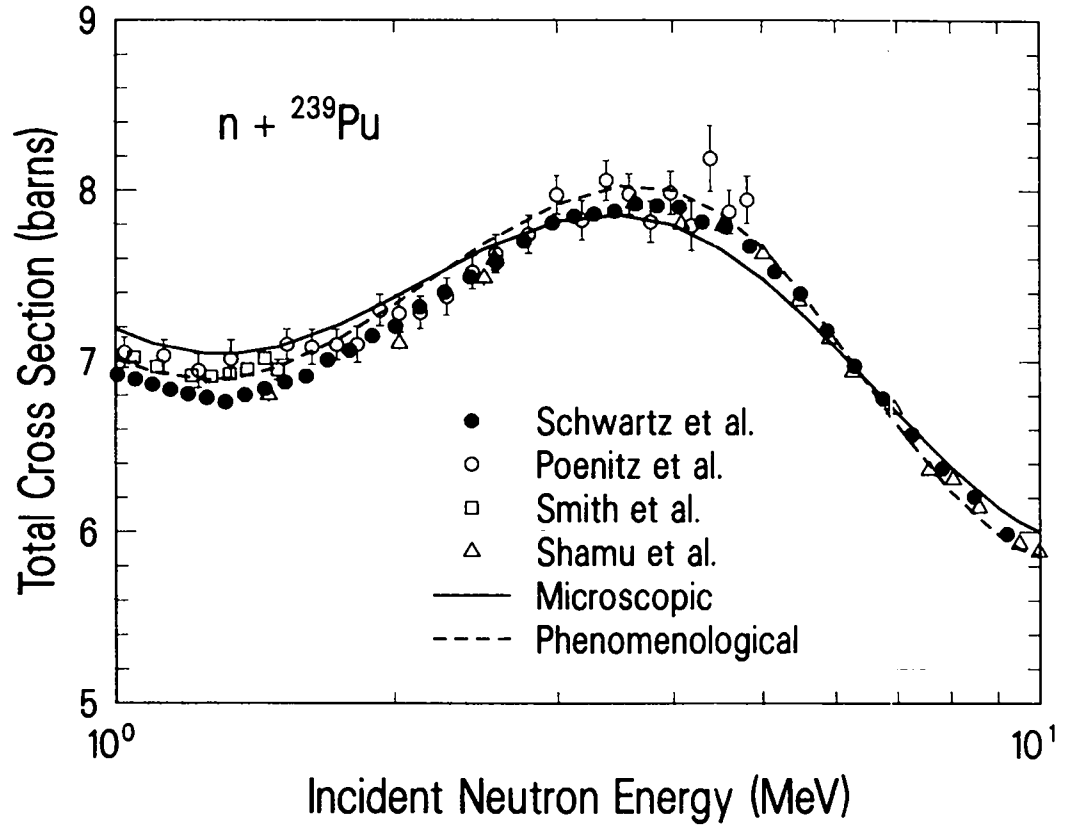

Fig. 15. Comparisons of calculated and experimental total cross sections for n + ^{239}Pu scattering over the incident neutron energy range 1 MeV $\leqq E_n \leqq$ 10 MeV.

J. Differential and Integral Comparisons of Three Representations of the Prompt Neutron Spectrum for the Spontaneous Fission of ^{252}Cf [D. G. Madland, R. J. LaBauve, and J. R. Nix (T-9)]

Because of their importance as neutron standards, we present comparisons of measured and calculated prompt fission neutron spectra N(E) and average prompt neutron multiplicities $\bar{\nu}_p$ for the spontaneous fission of ^{252}Cf. In particular, we test three representations of N(E) against recent experimental measurements of the differential spectrum and threshold integral cross sections. These representations are the Maxwellian spectrum, the NBS spectrum,[29,30] and the Los Alamos spectrum of Madland and Nix.[31,32] For the Maxwellian spectrum, we obtain the value of the Maxwellian temperature T_M by a least squares adjustment to the experimental differential spectrum of Poenitz and Tamura.[33] For the Los Alamos spectrum, a similar least squares adjustment determines the nuclear level-density parameter a, which is the single unknown parameter that appears. The NBS spectrum has been previously constructed by adjustments to eight differential spectra measured during the period 1965 to 1974. Among these three representations, we find that the Los Alamos spectrum best reproduces both the differential and integral measurements, assuming ENDF/B-V cross sections in the calculation of the latter. Although the NBS spectrum reproduces the integral measurements fairly well, it fails to satisfactorily reproduce the new differential measurement, and the Maxwellian spectrum fails to satisfactorily reproduce the integral measurements. Additionally, we calculate a value of $\bar{\nu}_p$ from the Los Alamos theory that is within approximately 1% of experiment.

DIFFERENTIAL COMPARISONS

We compare the three representations of the prompt fission neutron spectrum that we are studying with each other and with a recent high quality differential measurement of the spectrum. In fact, because of the use of the ^{252}Cf(sf) spectrum as a standard, we determine the Maxwellian temperature T_M by a least squares adjustment to the experimental spectrum instead of by other means and, for the identical reason, we determine the nuclear level-density parameter a for the Los Alamos spectrum in the same way. The NBS spectrum, with twelve parameters, has been previously obtained by least squares adjustments and therefore is already completely determined.

For our present purposes, we choose the recent differential spectrum measurement of Poenitz and Tamura[33] as our experimental reference spectrum.

This experiment covers a secondary neutron energy range of 0.225 to 9.8 MeV with 51 points that represent approximately 95% of the total spectrum. The average experimental uncertainty in the set of 51 points is 3.6%.

1. Maxwellian Spectrum.

The least squares adjustment of the Maxwellian spectrum to the experimental reference spectrum is performed with respect to the Maxwellian temperature parameter T_M. To obtain an absolute value of χ^2 per degree of freedom, the normalization of the experiment is recomputed for each iteration in the value of T_M. We find a minimum in χ^2, $\chi^2(\text{min}) = 1.201$, at a value of $T_M = 1.429$ MeV. This value yields mean and mean-square energies of the Maxwellian spectrum of 2.144 MeV and 7.658 MeV^2, respectively. These values are also given in Table IV together with other properties of the Maxwellian spectrum.

TABLE IV

SOME PROPERTIES OF THREE REPRESENTATIONS OF THE PROMPT NEUTRON SPECTRUM FOR THE SPONTANEOUS FISSION OF ^{252}Cf

Quantity	Maxwellian	NBS	Los Alamos
Physical shape	smooth	five-segment piecewise continuous	smooth
Number of explicit parameters	1	12	3
Number of least-squares adjusted parameters in the present work	1	0	1
Adjusted Maxwellian temperature T_M (MeV)	1.429	—	—
Adjusted nuclear level-density parameter a (1/MeV)	—	—	A/9.15
$\langle E \rangle$ (MeV)	2.144	2.120	2.134
$\langle E^2 \rangle$ (MeV^2)	7.658	7.433	7.364
$\bar{\nu}_p$	—	—	3.810
χ^2 (min)	1.201	1.922[a]	0.552

[a] In this case, χ^2 (min) is the only value of χ^2 and it is calculated assuming zero degrees of freedom.

The spectrum is compared with the experimental spectrum in Fig. 16 in absolute units, as well as in Fig. 17 where the ratio of the experimental spectrum to this spectrum is plotted. The highest energy experimental points on Fig. 16 indicate that perhaps the Maxwellian spectrum is slightly larger than experiment in this region. Inspection of Fig. 17 confirms this for energies greater than about 5 MeV, with departures from experiment that are perhaps as large as 10%. In addition, one sees that the Maxwellian spectrum is larger than experiment by 2-7% in the region below 0.4 MeV and that it is smaller by 2-5% in the region between 1.5 and 3.0 MeV. At high energy, despite the adjustment of T_M with respect to experiment, the Maxwellian spectrum is still somewhat greater than experiment, reflecting a fundamental difficulty in accounting for two physical effects with a single parameter.

2. NBS Spectrum.

The comparison of this spectrum with the experimental differential spectrum is shown in Fig. 16 in absolute units, and in Fig. 17, where the ratios of this spectrum and the experimental spectrum to the least squares adjusted Maxwellian spectrum are shown. The computed value of χ^2 per degree of freedom for this previously determined spectrum is 1.922. The mean and mean-square energies are listed in Table IV together with other properties of the NBS spectrum.

Figures 16 and 17 both indicate that the NBS spectrum agrees with the experimental reference spectrum in the high energy region better than the least squared adjusted Maxwellian spectrum. On the other hand, the NBS spectrum lies about 5-15% above experiment at energies below 0.5 MeV, giving rise to the factor of 2 deterioration in the value of χ^2 per degree of freedom relative to that of the least squares adjusted Maxellian spectrum. In the region between 0.8 and 3.0 MeV, the NBS and adjusted Maxwellian spectra behave similarly, with departures from experiment ranging from 1 to 5%. Neither representation reproduces the structure in the experimental spectrum between 1.5 and 3.0 MeV.

3. Los Alamos Spectrum.

The least squares adjustment of the Los Alamos spectrum to the experimental differential spectrum is performed with respect to the nuclear level-density parameter a. As before, to obtain an absolute value of χ^2 per degree of freedom, the normalization of the experiment is recomputed for each iteration

in the value of a. We find a minimum in χ^2, $\chi^2(\text{min}) = 0.552$, at a value of a = A/9.15(MeV). The values of the mean and mean-square energies are listed in Table IV where they may be compared with the corresponding values from the Maxwellian and NBS spectra. The spectrum itself is compared with the experimental differential spectrum in Figs. 16 and 17.

Figure 16 shows that the Los Alamos spectrum is somewhat less than experiment at the two highest energy experimental points. However, as shown by Fig. 17, the uncertainties in these two data points are too large to draw any certain conclusion. Figure 17 shows that the shape and magnitude of the Los Alamos spectrum agrees very well with experiment over the entire range, except for the region below 0.5 MeV where the experiment is under-predicted by amounts ranging from 1 to 5%.

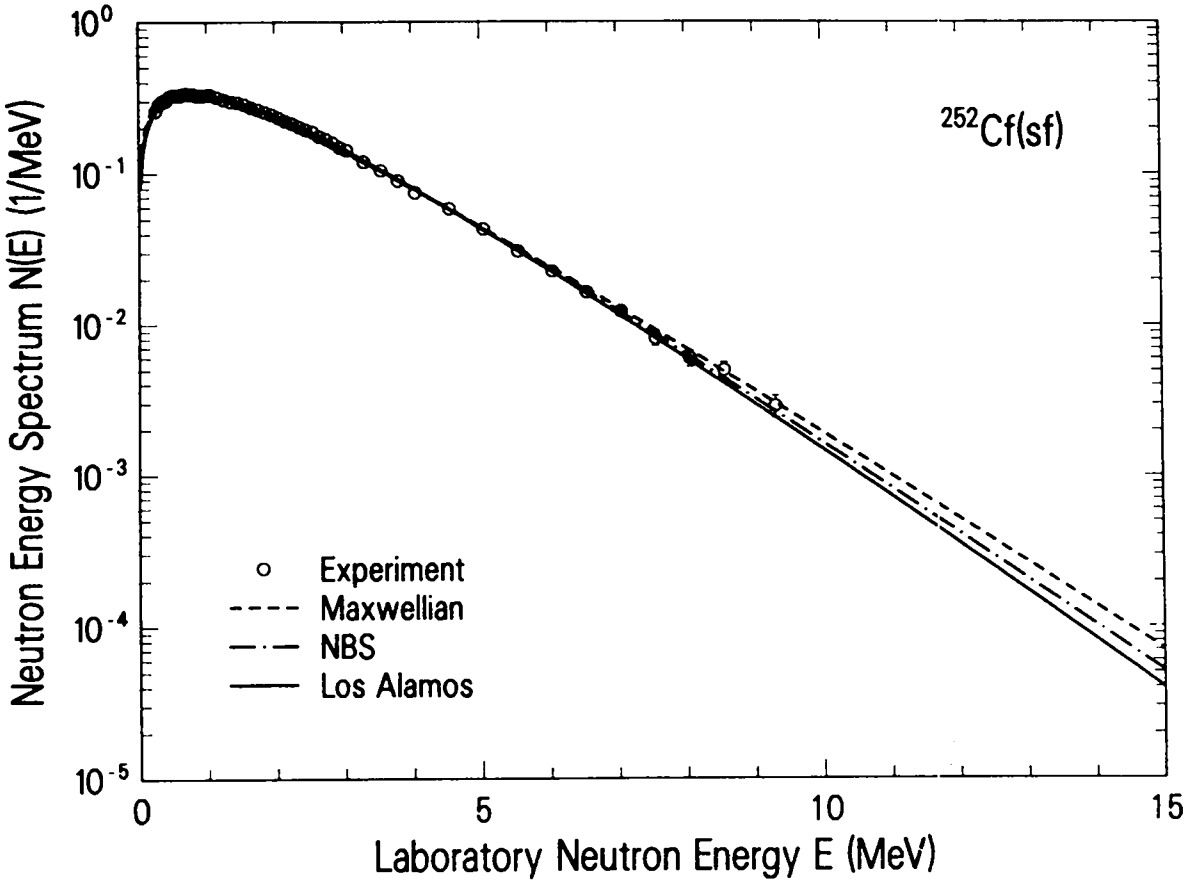

Fig. 16. Prompt fission neutron spectrum in the laboratory system for the spontaneous fission of ^{252}Cf. The dashed curve gives the least-squares adjusted Maxwellian spectrum, the dot-dashed curve gives the NBS spectrum, and the solid curve gives the least squares adjusted Los Alamos spectrum. The experimental data are those of Poenitz and Tamura (Ref. 33).

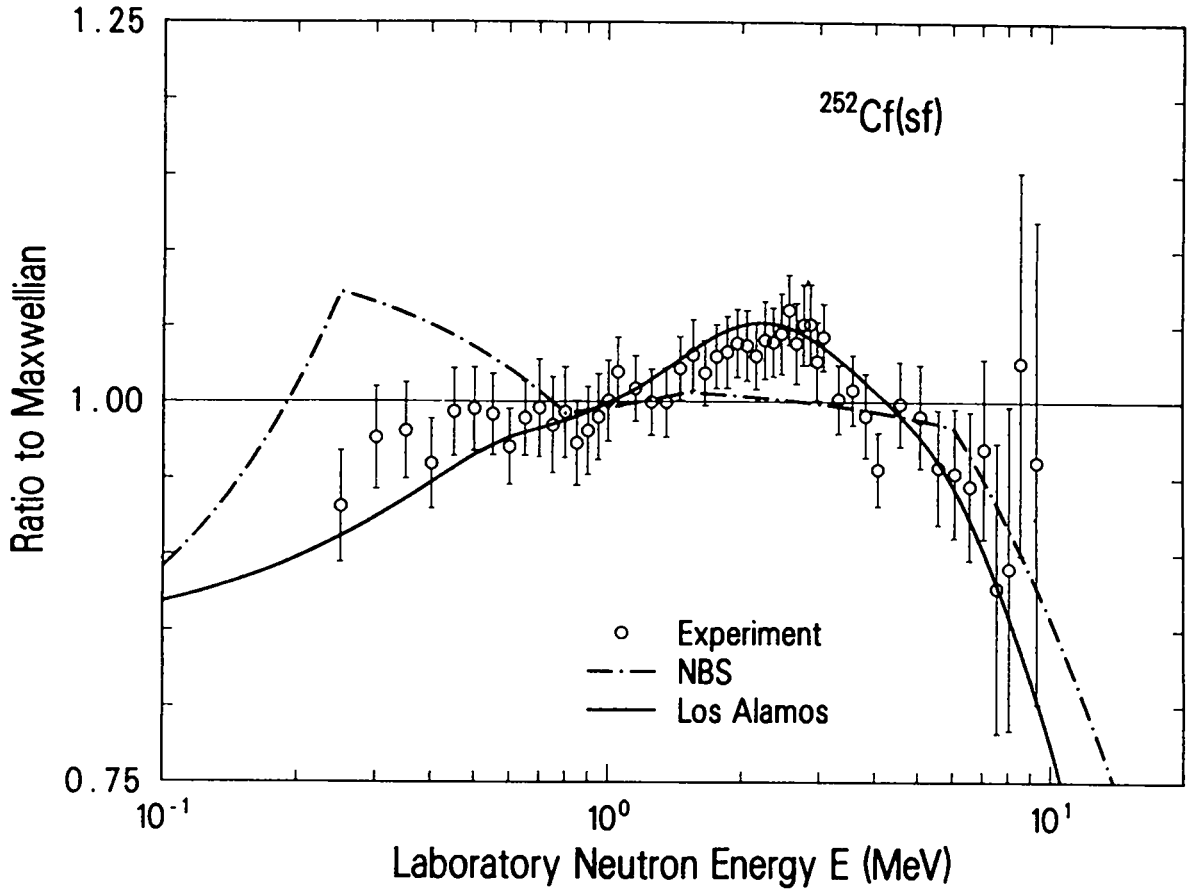

Fig. 17. Ratio of the NBS spectrum, the least squares adjusted Los Alamos spectrum, and the experimental spectrum to the least squares adjusted Maxwellian spectrum, corresponding to the curves shown in Fig. 16.

The value of the nuclear level-density parameter a = A/9.15(MeV) obtained in our least squares adjustment also provides for the calculation of $\bar{\nu}_p$ = 3.810. This value is within 1.4% of the experimental value of 3.757 ± 0.009 obtained from the measurements of Amiel[34] and Smith,[35] and is within 1.0% of the experimental value of 3.773 ± 0.007 obtained by Spencer et al.[36]

Figure 17 clearly shows that the Los Alamos spectrum is the preferred representation for the present choice of the Poenitz and Tamura[33] experimental reference differential spectrum. This conclusion is reinforced by comparing the values of χ^2 per degree of freedom from Table IV. These show the Los Alamos spectrum to be the preferred representation by a factor ~ 3 over the NBS spectrum and by a factor ~ 2 over the Maxwellian spectrum. In addition to having the poorest agreement with the experimental differential spectrum, the NBS spectrum is somewhat unphysical in that it is only piecewise continuous.

INTEGRAL COMPARISONS

We calculate fifteen threshold integral cross sections for each of the three representations of the prompt fission neutron spectrum that we are studying and compare our results with recent high-quality experimental measurements carried out by Grundl et al.[37] and Kobayashi et al.[38,39] We also compare the trends of each of the three sets of calculated integral cross sections to assess the overall quality of the three spectrum representations being used. This latter comparison is, of course, only possible if identical pointwise cross sections are used in each set of calculations.

For purposes of graphical presentation and discussion of our results, we define an effective threshold energy, E_{th}, for each reaction studied, as the energy that divides the pointwise cross-section integral at 0.01% and 99.99%. We use the ratio C/E of calculated integral cross sections to experimental integral cross sections as a function of E_{th} in the graphical presentation of our results that we now discuss.

1. Maxwellian Spectrum.

Our results for the least squares adjusted Maxwellian spectrum are given in the fourth column of Table V where they can be compared directly with the experimental results in the third column, and in Fig. 18 where the C/E values are plotted as a function of the threshold energy E_{th}. There are three points to mention. First, Table V shows that for a given set of pointwise cross sections and the Maxwellian spectrum, seven of the fifteen calculations are outside of the two-sigma measurement uncertainty. Second, nine of the fifteen calculations are outside of the one-sigma measurement uncertainty. Third, the trend of the C/E ratios shown in Fig. 18 indicates that the accuracy of the Maxwellian spectrum is increasingly worse with increasing reaction threshold. That is, the Maxwellian spectrum is too large (hard) in the high energy portion of the spectrum. This result is consistent with our conclusions for the differential spectrum comparisons. As already discussed, this illustrates a fundamental difficulty in accounting for two physical effects with a single parameter.

2. NBS Spectrum.

Our results for the NBS spectrum are given in the fifth column of Table V and are illustrated in Fig. 18. Again, there are three points to be made. First, Table V shows for the identical set of pointwise cross sections and the NBS spectrum, only four of fifteen calculations are outside of the two-sigma

measurement uncertainty. Second, only seven of the fifteen calculations are outside of the one-sigma measurement uncertainty. Third, the trend of the C/E ratios shown in Fig. 18 indicates that the NBS spectrum reproduces the experimental integral cross sections reasonably well for most values of the threshold energy.

TABLE V

COMPARISON OF MEASURED AND CALCULATED INTEGRAL CROSS SECTIONS FOR THREE REPRESENTATIONS OF THE PROMPT NEUTRON SPECTRUM FOR THE SPONTANEOUS FISSION OF ^{252}Cf†

Reaction	E_{th} (MeV)	Measurement[a]	Maxwellian Calc.	Maxwellian (C/E)	NBS Calc.	NBS (C/E)	Los Alamos Calc.	Los Alamos (C/E)
$^{235}U(n,f)$	0.00	1216.0 ± 19.46	1238.657	(1.019)	1235.918	(1.016)	1235.720	(1.016)
$^{115}In(n,n')$	0.76	201.0 ± 8.2	182.804	(0.909)*	181.936	(0.905)*	186.009	(0.925)
$^{58}Ni(n,p)$	0.80	118.5 ± 4.1	115.888	(0.978)	113.891	(0.961)	114.039	(0.962)
$^{47}Ti(n,p)$	1.14	21.58 ± 1.16	24.463	(1.134)*	24.070	(1.115)*	24.209	(1.122)*
$^{54}Fe(n,p)$	1.36	87.63 ± 4.35	89.968	(1.027)	88.346	(1.008)	88.323	(1.008)
$^{32}S(n,p)$	1.80	72.52 ± 2.96	72.665	(1.002)	71.447	(0.985)	71.662	(0.988)
$^{27}Al(n,p)$	2.86	4.891 ± 0.179	5.375	(1.099)*	5.140	(1.051)	4.967	(1.016)
$^{46}Ti(n,p)$	2.97	14.04 ± 0.61	14.080	(1.003)	13.474	(0.960)	13.014	(0.927)
$^{51}V(n,p)$[b]	3.41	0.713 ± 0.059	0.732	(1.027)	0.688	(0.966)	0.657	(0.921)
$^{56}Fe(n,p)$	4.65	1.440 ± 0.070	1.546	(1.073)	1.416	(0.983)	1.322	(0.918)
$^{48}Ti(n,p)$	5.07	0.415 ± 0.016	0.460	(1.107)*	0.410	(0.986)	0.377	(0.907)*
$^{59}Co(n,\alpha)$	5.52	0.218 ± 0.014	0.243	(1.115)	0.217	(0.997)	0.200	(0.919)
$^{24}Mg(n,p)$	5.58	1.940 ± 0.093	2.404	(1.239)*	2.159	(1.113)*	1.995	(1.028)
$^{27}Al(n,\alpha)$	5.71	1.006 ± 0.022	1.195	(1.187)*	1.060	(1.053)*	0.973	(0.967)
$^{197}Au(n,2n)$	8.31	5.267 ± 0.226	6.817	(1.294)*	5.650	(1.073)	4.973	(0.944)

† Using ENDF/B-V pointwise cross sections, unless otherwise noted, and expressing the results in millibarns.

* Calculation outside two-sigma measurement uncertainty.

[a] The experimental measurements are those of Grundl et al (Ref. 37) and Kobayashi et al. (Refs. 38 and 39).

[b] The pointwise cross section used in the calculation for this reaction is from Smith et al. (Ref. 40).

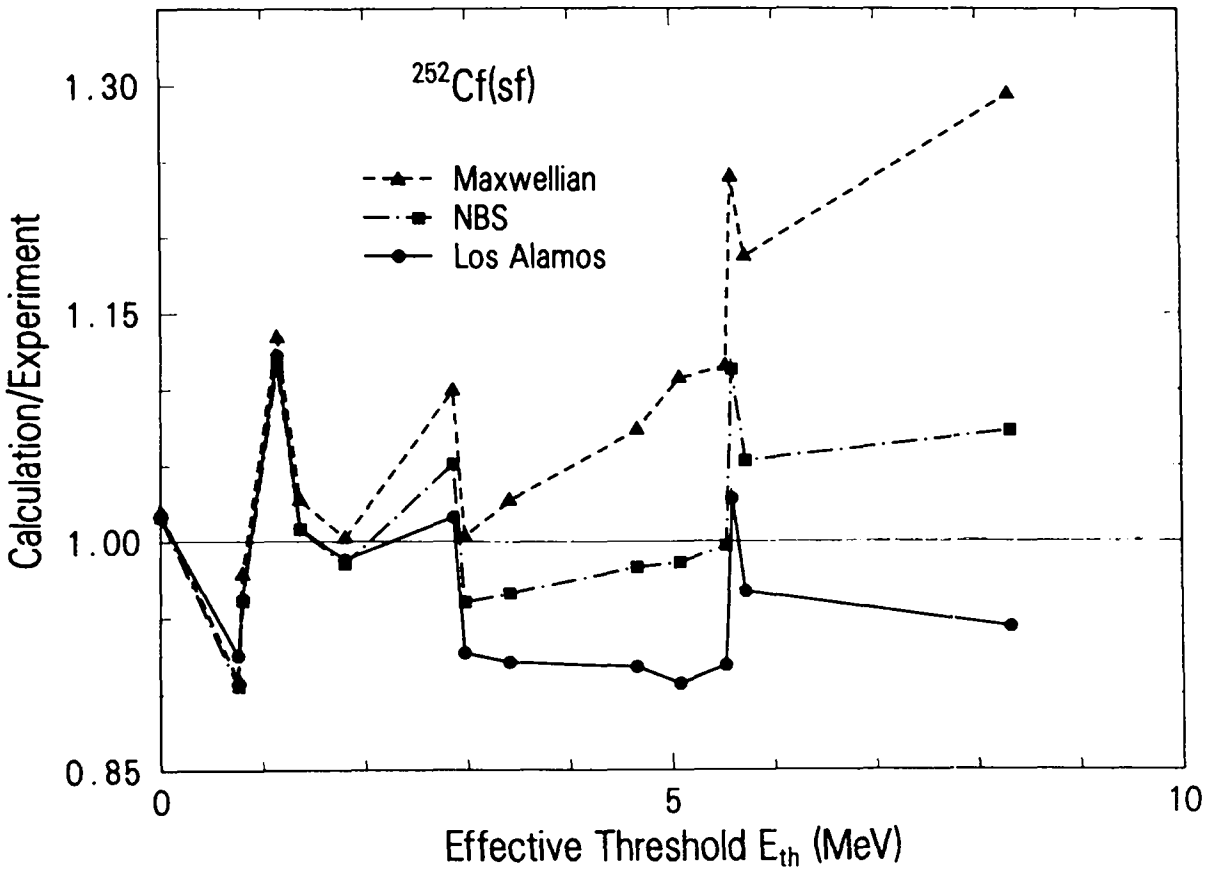

Fig. 18. Ratio of calculated to experimental integral cross sections for the prompt neutron spectrum from the spontaneous fission of ^{252}Cf as a function of the effective neutron threshold energy for the reaction. The calculated values are obtained using the spectra discussed in the text together with ENDF/B-V pointwise cross sections. The experimental values are those of Grundl et al. (Ref. 37) and Kobayashi et al. (Refs. 38 and 39). The dashed, dot-dashed, and solid lines serve as guides to the eye.

3. Los Alamos Spectrum.

Our results for the Los Alamos spectrum are given in the last column of Table V and are illustrated in Fig. 18. Once again, there are three points to address. First, Table V shows that, for the identical set of pointwise cross sections and the Los Alamos spectrum, only two of the fifteen calculations are outside of the two-sigma measurement uncertainty. Second, nine of the fifteen calculations are outside of the one-sigma measurement uncertainty. Third, the trend of the C/E ratios shown in Fig. 18 indicates that the Los Alamos spectrum, like the NBS spectrum, reproduces the experimental integral cross sections reasonably well for most values of the threshold energy.

Figure 18 clearly shows that the least squares adjusted Maxwellian spectrum is unsatisfactory when using the present choice of the Poenitz and Tamura[33] experiment to determine the Maxwellian temperature T_M = 1.429 MeV. Although we do not show the results here, this same conclusion is obtained when using the popular value T_M = 1.42 MeV. Finally, the figure also indicates, on the basis of the chosen set of experimental integral cross sections, that the NBS and the Los Alamos spectra could each be adjusted somewhat, were it not for the constraints imposed by the experimental differential spectrum measurements.

On the basis of the comparisons presented here, we conclude that the Los Alamos spectrum is the preferred representation of N(E) because it best reproduces both the differential and integral measurements, assuming ENDF/B-V cross sections in the calculation of the latter. Although the NBS spectrum reproduces the integral measurements fairly well, it fails to satisfactorily reproduce the recent differential measurements, and the Maxwellian spectrum fails to satisfactorily reproduce the recent integral measurements. Additionally, we calculate a value of $\bar{\nu}_p$ from the Los Alamos theory that is within approximately 1% of experiment. In this study we have learned that well-measured high-threshold integral cross sections provide valuable constraints on the differential spectrum, assuming the pointwise cross sections are well known. Finally, we mention that the Los Alamos spectrum has been adopted as the preliminary standard spectrum for ENDF/B-VI. The spectrum is available in tabular form from the US National Nuclear Data Center, Brookhaven National Laboratory.

K. Calculation of Average Pairing Gaps [D. G. Madland and J. R. Nix (T-9)]

This work is continuing. We are presently installing the most recent compilation[41] of experimental and systematic masses into our Fortran code PAIR. This code calculates Δ_n, Δ_p, and Δ from these masses as well as from various model assumptions that we are testing.

L. Medium Energy Proton-Nucleus Scattering Calculations (D. G. Madland)

This work is continuing. At the present time the Dirac phenomenological approach is under study for both low and medium energy proton-nucleus scattering. Particular attention is being given to the calculation of the total reaction cross section.

II. NUCLEAR CROSS-SECTION PROCESSING AND TESTING

A. Monte-Carlo Cross Sections [R. E. MacFarlane and R. C. Little (X-6)]

Cross sections for the continuous-energy Monte-Carlo transport code MCNP are normally prepared using the ACER module of NJOY. Two major changes have been made to ACER recently, namely, Type-1 output and LAW 4 neutron emission.

Because of the worldwide interest in MCNP, Group X-6 has put a lot of effort into developing a transportable version based on FORTRAN-77. Although the distribution package for MCNP-3 includes a quite usable cross-section library, many users will need to be able to process their own libraries from new or modified evaluations in ENDF format. Therefore, we have updated the ACER module to produce the latest version of the transportable, formatted (i.e., BCD, ASCII, EBCDIC, etc.), "Type-1" output. This update required two small changes to the ACER input instructions. First, the user must specify a unit number for MCNP directory, "NDIR." The second input change is to specify "NTYPE," which defines the output format desired. The locations of these input changes are given in the comment cards at the start of the ACER module. After the run is complete, the user must change "FILENAME ROUTE" in the directory file to provide a retrieval path for the data file. For thermal libraries, the third line of the ACE file must be modified to contain ZA identifiers of the isotopes for which the thermal data are appropriate.

In the current version of MCNP, tabulated neutron secondary energy distributions (LAW=1) are sampled by using 32 equally probable bins. The method is efficient and compact, but, as suggested by Fig. 19, it can produce significant errors for very low or very high secondary energies. As more detailed tabulated spectra become common in ENDF/B evaluations, it has become important to provide a more accurate sampling procedure. Therefore, we have modified ACER to generate cumulative probability distributions for secondary neutrons using the "LAW=4" format originally introduced for photon emission. A companion 10-line update to MCNP is available that uses the new law.

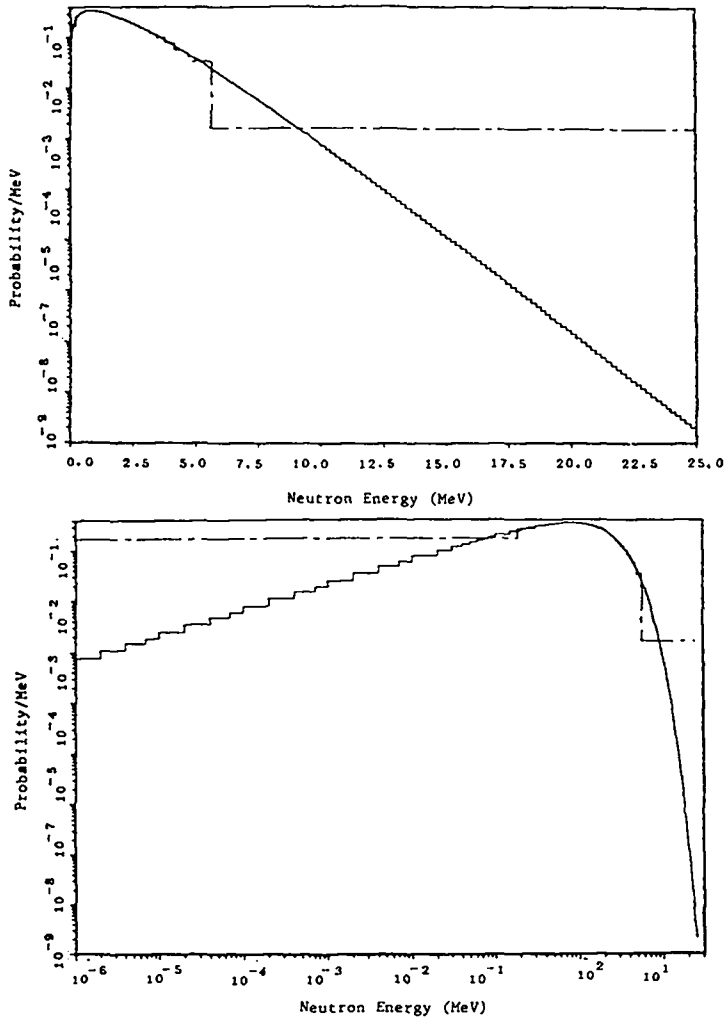

Fig. 19. Fission spectrum for ^{237}Np induced by neutrons with an energy of 1×10^{-5} eV (solid) compared with 32-bin representation previously used by MCNP (chain dash). The upper figure emphasizes high energies and the lower one emphasizes low energies.

B. Charged Particle Experimental Data [R. MacFarlane, G. Hale, L. Stewart (X-6), R. Howerton and S. T. Perkins (Lawrence Livermore National Lab.)]

The Experimental Cross-Section Information Library (ECSIL)[42] was originally developed at the Lawrence Livermore National Laboratory (LLNL) for indexing and retrieving the experimental neutron cross-section data needed in the evaluation process, and it has also been in use by Group T-2 for this purpose for many years. We are now engaged in a joint program with LLNL to produce ECSIL2. This new system will also be useful for charged-particle data and will run efficiently on the CRAY1 computers used at both laboratories.

The ECSIL2 system has four components: an experimental data file, a directory file, a bibliography file, and a set of utility codes.

The data file uses a random access structure, and includes formats for all the most useful types of measurements (e.g., integrated cross sections, angular distributions, energy distributions, polarizations, etc.). The initial data file has been drawn from two sources. First, there is the extensive elastic scattering data described in Ref. 43; and second, there is the cross section and polarization data gathered by Group T-2 for the R-matrix code EDA. These two sources combined yield approximately 25 500 data points. Additional data will be added in the process of evaluating other cross sections. Contributions are welcome (and hereby solicited).

The directory file contains an entry for each data set keyed by parameters such as projectile, target, reaction, and energy range. Each entry also has a pointer to the corresponding entry in the data file and the bibliographic reference. This directory can be searched and sorted in various ways to find desired data. Two common indexes are ZA order and reference order, as demonstrated in Tables V and VI, respectively.

TABLE V

PART OF A TYPICAL ZA-ORDERED INDEX FOR AN ECSIL2 LIBRARY[a]

Z	A	YI	C	S	YO	I	ST	YR	REF	REACTION	X1	MEASUREMENT	X2	ENERGY RANGE		POINTS
1001	2	2	0	2	2	0	64	2151	1001 + P ELASTIC			XS(MU)		3.377-1	4.052-1	5
1001	2	2	0	2	2	0	66	575	1001 + P ELASTIC			XS(MU)		1.397+0	3.037+0	50
1001	2	2	0	2	2	0	75	519	1001 + P ELASTIC			XS(MU)		4.978+0	8.030+0	51
1001	2	2	0	2	2	0	76	2149	1001 + P ELASTIC			XS(MU)		5.957+0	1.360+1	97
1001	2	2	0	2	2	0	68	582	1001 + P ELASTIC			XS(MU)		6.141+0	8.097+0	33
1001	2	2	0	2	2	0	59	2141	1001 + P ELASTIC			XS(MU)		9.680+0	9.680+0	1
1001	2	2	0	2	2	0	59	581	1001 + P ELASTIC			XS(MU)		9.690+0	9.690+0	26
1001	2	2	0	2	2	0	71	579	1001 + P ELASTIC			XS(MU)		9.690+0	1.360+1	26
1001	2	2	0	2	2	0	68	2143	1001 + P ELASTIC			XS(MU)		1.416+1	1.416+1	17
1001	2	2	0	2	2	0	54	536	1001 + P ELASTIC			XS(MU)		1.820+1	1.820+1	8
1001	2	2	0	2	2	0	74	515	1001 + P ELASTIC			XS(MU)		1.970+1	1.970+1	13
1001	2	2	0	2	2	0	60	2146	1001 + P ELASTIC			XS(MU)		2.563+1	2.563+1	22
1001	2	2	0	2	11	0	59	2145	1001 + P ELASTIC			POL(MU)	2000	1.620+1	1.620+1.	1
1001	2	2	0	2	11	0	68	2143	1001 + P ELASTIC			POL(MU)	2000	2.020+1	2.020+1	8
1001	2	2	0	2	11	0	67	2142	1001 + P ELASTIC			POL(MU)	2020	1.140+1	2.650+1	4
1001	2	2	0	2	11	0	67	2147	1001 + P ELASTIC			POL(MU)	2020	2.700+1	2.700+1	1
1001	2	2	0	2	11	0	61	2148	1001 + P ELASTIC			POL(MU)	100·1000	2.760+1	2.760+1	2
1001	2	2	0	2	11	0	67	2142	1001 + P ELASTIC			POL(MU)	10100000	1.140+1	2.650+1	4
1001	2	2	0	2	11	0	75	2140	1001 + P ELASTIC			POL(MU)	200000000	1.000+1	1.000+1	7
1001	2	2	0	2	11	0	75	2144	1001 + P ELASTIC			POL(MU)	200000000	1.600+1	1.600+1	9
1001	2	2	0	2	11	0	61	2148	1001 + P ELASTIC			POL(MU)	300·1000	2.760+1	2.760+1	3

[a] This example is from the EDA data.

The bibliography file contains author names, source references, and sometimes special comments. References are correlated with data sets using unique 5-digit reference numbers. Bibliography listings can be generated in reference-number order, alphabetically by source name (journal, conference, book, etc.), alphabetically by author name (with cross references to every paper by that author), or by reference "tag" (first two letters of first author's last name plus last two digits of the publication date; e.g., AB85). Examples of reference-ordered, author-ordered, and tag-ordered bibliographies are shown in Tables VII, VIII, and IX. The current bibliography file is a combination of

TABLE VI

PART OF A TYPICAL REFERENCE-ORDERED INDEX FOR AN ECSIL2 LIBRARY[a]

REF	ST	YR	Z	A	YI	C	S	YO	I	REACTION	X1	MEASUREMENT	X2	ENERGY	RANGE	POINTS
2092	0	70	1003	3	11	0	1	11		1003 (D,N) 2004		POL(MU)	0	3.900+0	1.500+1	0
2093	0	71	1003	3	11	0	1	11		1003 (D,N) 2004		POL(MU)	0	6.000+0	1.000+1	0
2094	0	67	1003	3	11	0	1	11		1003 (D,N) 2004		POL(MU)	0	2.100+0	2.900+0	0
2095	0	76	1003	3	2	0	3	11		1003 + D ELASTIC		POL(MU)	0	1.050+1	1.050+1	0
2095	0	76	1003	3	34	0	6	11		1003 (D,A) 1		POL(MU)	0	1.050+1	1.050+1	0
2096	0	84	1002	4	11	0	0	0		1002 (T,N) 2004		INT.XS		1.250-2	1.170-1	0
2097	0	70	1003	3	11	0	1	11		1003 (D,N) 2004		POL(MU)	0	4.000-1	4.000-1	0
2098	0	70	1003	3	34	0	6	11		1003 (D,A) 1		POL(MU)	0	5.100-2	9.300-2	0
2100	0	79	1003	3	11	1	1	2		1003 (D,N) 2004	2.020+1	XS(MU)		4.800+0	8.330+0	0
2101	0	70	2003	2	2	0	2	11		2003 + P ELASTIC		POL(MU)	0	4.000+0	1.100+1	0
2102	0	69	2003	2	2	0	2	11		2003 + P ELASTIC		POL(MU)	0	4.000+0	1.100+1	0
2103	0	71	2003	2	2	0	2	11		2003 + P ELASTIC		POL(MU)	0	1.940+1	1.940+1	0
2104	0	73	1002	3	26	0	2	11		1002 (D,P) 1003		POL(MU)	0	6.000+0	1.500+1	0
2105	0	74	2003	2	2	0	2	11		2003 + P ELASTIC		POL(MU)	0	1.050+1	1.050+1	0
2106	0	76	2003	2	2	0	2	11		2003 + P ELASTIC		POL(MU)	0	2.300+0	8.800+0	0
2107	0	73	2003	2	2	0	2	11		2003 + P ELASTIC		POL(MU)	0	1.623+1	1.623+1	0
2108	0	79	2003	2	2	0	2	11		2003 + P ELASTIC		POL(MU)	0	1.750+0	4.500+0	0
2109	0	73	2003	2	2	0	2	11		2003 + P ELASTIC		POL(MU)	0	6.800+0	6.800+0	0
2110	0	78	2003	2	2	0	2	11		2003 + P ELASTIC		POL(MU)	0	6.820+0	1.077+1	0
2111	0	70	2003	2	2	0	2	11		2003 + P ELASTIC		POL(MU)	0	1.240+1	1.620+1	0
2112	0	71	2003	2	2	0	2	11		2003 + P ELASTIC		POL(MU)	0	1.360+1	1.360+1	0
2113	0	71	2003	2	2	0	2	2		2003 + P ELASTIC		XS(MU)		1.800+1	1.800+1	0
2114	0	65	3007	6	34	1	6	2		3007 (A,A) 3007		XS(MU)		4.390+0	5.920+0	0
2114	0	65	3007	6	34	1	6	2		3007 (A,A) 3007	4.776-1	XS(MU)		4.390+0	5.920+0	0
2115	0	79	1003	3	11	0	1	11		1003 (D,N) 2004		POL(MU)	0	3.000+0	6.000+0	0
2116	0	74	1003	3	11	0	1	11		1003 (D,N) 2004		POL(MU)	0	7.000+0	7.000+0	0
2117	0	66	2003	2	2	0	2	11		2003 + P ELASTIC		POL(MU)	0	1.620+1	1.970+1	0
2118	0	62	1003	4	11	0	0	0		1003 (T,N) 2005		INT.XS		6.000-2	1.150+0	0
2119	0	77	2004	4	2	0	4	2		2004 + T ELASTIC		XS(MU)		7.600+0	1.000+1	0
2119	0	77	2004	4	2	0	4	11		2004 + T ELASTIC		POL(MU)	0	7.600+0	1.000+1	0
2120	0	80	2004	4	2	0	4	2		2004 + T ELASTIC		XS(MU)		6.000+0	1.400+1	0
2120	0	80	2004	4	2	0	4	11		2004 + T ELASTIC		POL(MU)	0	6.000+0	1.400+1	0
2121	0	82	2004	4	11	0	1	2		2004 (T,N) 3006		XS(MU)		8.745+0	1.289+1	0
2121	0	82	2004	4	11	1	1	2		2004 (T,N) 3006	2.186+0	XS(MU)		8.745+0	1.289+1	0
2122	0	76	2004	4	2	0	4	3		2004 + T ELASTIC		EX.FUNCT.		8.500+0	9.050+0	0
2123	0	75	1002	3	11	0	1	11		1002 (D,N) 2003		POL(MU)	0	1.100+0	5.450+0	0
2124	0	84	2003	2	2	0	2	11		2003 + P ELASTIC		POL(MU)	0	2.140+1	4.960+1	0
2125	0	84	2003	2	2	0	2	2		2003 + P ELASTIC		XS(MU)		1.950+1	4.750+1	0
2126	0	84	6012	4	2	0	4	2		6012 + T ELASTIC		XS(MU)		9.000+0	1.100+1	0
2126	0	84	6012	4	2	0	4	11		6012 + T ELASTIC		POL(MU)	0	9.000+0	1.100+1	0
2127	0	83	1001	3	11	0	1	2		1001 (D,N) 2002		XS(MU)		4.280+1	4.280+1	0
2128	0	83	2004	3	54	0	0	0		2004 (D,PA) 1		INT.XS		1.200+1	1.700+1	0
2131	0	81	4009	4	34	1	6	2		4009 (T,A) 3008	6.530+0	XS(MU)		1.700+1	1.700+1	0
2131	0	81	4009	4	34	1	6	11		4009 (T,A) 3008	6.530+0	POL(MU)	0	1.700+1	1.700+1	0
2132	0	81	1001	3	26	0	2	11		1001 (D,P) 1002		POL(MU)	0	1.600+1	1.600+1	0
2133	0	79	1002	3	11	0	1	11		1002 (D,N) 2003		POL(MU)	0	1.550+1	1.700+1	0
2133	0	79	1002	3	26	0	2	11		1002 (D,P) 1003		POL(MU)	0	1.400+1	1.700+1	0
2134	0	79	4009	4	0	0	10	2		4009 (T		XS(MU)		1.700+1	1.700+1	0
2134	0	79	4009	4	0	0	10	11		4009 (T		POL(MU)	0	1.700+1	1.700+1	0
2135	0	77	2003	4	28	0	3	11		2003 (T,D) 2004		POL(MU)	0	9.000+0	1.700+1	0

[a] This example is from the master bibliography.

TABLE VII

PART OF A TYPICAL REFERENCE-ORDERED BIBLIOGRAPHY FOR AN ECSIL2 LIBRARY[a]

REF	BIBLIOGRAPHY	REACTION	S	MEASUREMENT	ENERGY RANGE		POINTS
525	PHYS. REV. 87, 932 (1952) T.M.PUTNAM (U.C.BERKELEY)	2004 + P ELASTIC		XS(MU)	9.480+0	9.480+0	0
525	UCRL-1447 (1951)						
526	PHYS. REV. 88, 433 (1952) J.C.ALLRED, A.H.ARMSTRONG,	1002 + P ELASTIC		XS(MU)	9.700+0	9.850+0	0
526	R.O.BONDELID, L.ROSEN (LASL)						
527	PHYS. REV. 88, 1408 (1952) K.B.MATHER (WASHINGTON U.)	1001 + D ELASTIC		XS(MU)	1.020+1	1.020+1	0
		1002 + P ELASTIC		XS(MU)	5.100+0	5.100+0	0
528	PHYS. REV. 90, 899 (1953) H.R.WORTHINGTON, J.N.MCGRUER,	1001 + P ELASTIC		EX.FUNCT.	1.855+0	4.203+0	0
528	D.E.FINDLEY (UNIVERSITY OF WISCONSIN)						
529	PHYS. REV. 91, 438 (1953) G.R.BRIGGS, S.SINGER,	2004 + A ELASTIC		XS(MU)	2.180+1	3.000+1	0
529	W.K.JENTSCHKE (UNIVERSITY OF ILLINOIS)						
	DATA TAKEN FROM LA-2014 (1956)						
	PHYS. REV. 91, 438 (1953)						
530	PHYS. REV. 92, 660 (1953) F.E.STEIGEST, M.B.SAMPSON	2004 + A ELASTIC		XS(MU)	1.288+1	2.162+1	0
530	(INDIANA UNIVERSITY)						
	DATA NOT EXPERIMENTAL POINTS BUT ARE TAKEN FROM CURVES IN						
	LA-2014 (1956) SO THAT THEY ARE ROUGHLY LINEARLY INTERPOLABLE						
531	PHYS. REV. 92, 1501 (1953) T.LAURITSEN, T.HUUS,	2004 + D ELASTIC		EX.FUNCT.	1.000+0	1.200+0	0
531	S.G.NILSSON (DENMARK)						
532	PHYS. REV. 93, 825 (1954) G.FREIER, H.HOLMGREN	2003 + D ELASTIC		EX.FUNCT.	3.840-1	5.720-1	0
532	(UNIVERSITY OF MINNESOTA)	2003 (D,A) 1001		INT.XS	3.200-1	5.700-1	0
532	DATA TAKEN FROM LA-2014 (1956).						
533	PHYS. REV. 93, 837 (1954) W.E.KREGER, W.JENTSCHKE,	2004 + P ELASTIC		XS(MU)	5.780+0	5.780+0	0
533	P.G.KRUGER (UNIVERSITY OF ILLINOIS)						
534	PHYS. REV. 93, 928 (1954) K.F.FAMULARO, R.J.S.BROWN,	2003 + P ELASTIC		XS(MU)	8.200-1	3.520+0	0
534	H.D.HOLMGREN, T.F.STRATTON (UNIVERSITY OF MINNESOTA)						
	DATA TAKEN FROM LA-2014 (1956).						
535	PHYS. REV. 95, 772 (1954) M.E.ENNIS, A.HEMMENDINGER (LASL)	1003 + P ELASTIC		XS(MU)	9.900-1	2.548+0	0
536	PHYS. REV. 95, 1226 (1954) J.L.YNTEMA, M.G.WHITE	1001 + P ELASTIC		XS(MU)	1.800+1	1.800+1	0
536	(PRINCETON UNIVERSITY)						
537	PHYS. REV. 96, 1322 (1954) E.J.ZIMMERMAN, R.O.KERMAN,	1001 + P ELASTIC		XS(MU)	5.770+0	5.770+0	0
537	S.SINGER, P.G.KRUGER, W.JENTSCHKE (UNIVERSITY OF ILLINOIS)						
538	PHYS. REV. 98, 28 (1955) D.O.CALDWELL, J.R.RICHARDSON	1002 + P ELASTIC		XS(MU)	2.057+1	2.057+1	0
538	(U.C.L.A.)						
539	PHYS. REV. 100, 960 (1955) G.C.PHILLIPS, J.L.RUSSELL,	2004 + A ELASTIC		XS(MU)	2.960+0	5.764+0	0
539	C.W.REICH (RICE UNIVERSITY)						
	DATA OBTAINED FROM LA-2014 (1956).						
540	PHYS. REV. 128, 707 (1962) L.STEWART, J.E.BROLLEY,JR.,	2004 + D ELASTIC		XS(MU)	6.000+0	1.370+1	0

[a] This example is from the master bibliography.

TABLE VIII

PART OF A TYPICAL AUTHOR-ORDERED BIBLIOGRAPHY FOR AN ECSIL2 LIBRARY

AUTHOR	CITATIONS			
ABBONDANNO, U.	909*			
ABRAMOVICH, S.M.	21*			
ABRAMOVICH, S.N.	90*	94*	421*	845
	847	903		
AD'YASEVICH, B.P.	755*			
ADELBERGER, E.G.	101*	235*	368	956
	1006			
ADLOFF, J.C.	6*	41*		
ADYASEVICH, B.P.	2197*			
AGNEW, H.M.	703*	719		
AGUILAR, J.	983			
AHMED OSMAN	7*			
AJZENBERG-SELOVE, F.	50*	93*	95*	100*
	190*	1211*	1219*	1222
	1223*	2131		
AKIYAMA, M.	939			
AL'-DZHAUAKHIRI, A.U.	1039*			
ALBERT, R.D.	1134*			
ALBERTS, H.W.	648			
ALBURGER, D.E.	91*			
ALEKSIC, M.	348	1156		
ALEKSIC, M.R.	96*	488	1155	2058
ALESSI, V.E.	168			
ALEXANDER, T.K.	318	804	1203	
ALFORD, W.L.	825			
ALLAB, M.	19	857*		
ALLABY, J.V.	2148*			
ALLAN, D.L.	698*			
ALLAS, R.G.	135	741*	785*	
ALLEN, K.W.	92*	109*	258	
ALLEN, R.C.	60	591*	704	
ALLRED, J.C.	502	505*	506	524*
	526*	562*	680*	
ALMOND, P.R.	126*	653		
ALMQVIST, E.	92	109	258	881*
	1232*	1285		
ALSORAYA, A.M.	2020*			
AMBROSINO, G.	730*			
AMCHALI, F.	729			
AMES, O.	193*	196*		
AMMIRAJU, P.	1082*			
AMOKRANE, A.	71			
ANDERS, B.	350*	803*		
ANDERSON, A.N.	29			
ANDERSON, B.D.	183*	2119		
ANDERSON, J.D.	331	687	749	787
	978*	1135*	1136	2035
ANDRADE, E.	12*	415	2030	
ANDRE, G.O.	312*			
ANDREEV, G.B.	902*	1178*	1270*	
ANDREEV, M.F.	1057			
ANNEGARN, H.D.	824*			

AUTHOR	CITATIONS			
ANNEGARN, H.J.	1079*			
ANTONENKO, V.G.	755	2197		
ANTOUFIEV, Y.P.	356*			
ANTTILA, A.	789*	796*		
ARENA, N.	626*	925*		
ARGO, H.V.	570	703	719*	721
ARIFKHANOV, U.R.	99*	883*	977	
ARMITAGE, B.H.	2025			
ARMSTRONG, A.H.	505	526	716	
ARMSTRONG, D.D.	2104	2152	2171	2179
	2205	2212	2214	
ARMSTRONG, W.T.	2154			
ARNOLD, L.G.	808	2131*		
ARNOLD, W.	20	1302		
ARNOLD, W.R.	688*			
ARTEMOV, K.P.	97*	98*	601*	696*
	742*	1265*		
ARVIEUX, J.	61	70	2184*	
ASFOUR, F.	616	1151	1154	2048
	2055			
ASHMORE, A.	2148			
ASSIMAKOPOULOS, P.A.	602*	2010*	2036*	
AUCHAMPAUGH, G.F.	849			
AUDEBERT, B.	1045			
AUSTIN, S.M.	316*	756	891	981*
AUTON, D.L.	1199*			
AUWARTER, W.	353*			
AVER'YANOV, I.K.	1057			
AVES, R.	697			
AVIDA, R.	148			
AZIMOV, S.A.	977*			
AZUMA, R.E.	898	899	1298	
BABA, M.	469	939		
BACH, G.G.	1090*			
BACHER, A.D.	55*	65	77*	486
	510	585*	587*	
BADOVSKIV, V.P.	425			
BADRINATHAN, C.	231			
BAGGETT, L.M.	282*	283*		
BAHR, K.	1250*			
BAILEY, C.L.	567			
BAIR, J.K.	308*	684	1144	1220*
	2034			
BAIRD, S.	42			
BAKER, C.P.	93			
BAKER, M.P.	53*			
BAKER, S.D.	2101	2103*	2109	2154
	2191			
BALABANOV, E.M.	835*	836*		
BALAKRISHNAN, M.	277*			
BALASHKO, IU.G.	66*			
BALASHKO, YU.G.	67*	702*		

TABLE IX

PART OF A TYPICAL TAG-ORDERED BIBLIOGRAPHY FOR AN ECSIL2 LIBRARY

TAG	REF-N	REFERENCE
AB70	94	IZV.AKAD.NAUK SSSR (SER.FIZ.) 34, 1724
AB73	90	IZV.AKAD.NAUK SSSR (SER.FIZ.) 37, 1967
AB75	909	NUOVO CIMENTO 29, 187
AB79	21	YAD.FIZ. 30, 1276
AB80	421	YAD.FIZ. 32, 402
AD67	2197	SOV.J.NUCL.PHYS. 5, 665
AD69	235	NUCLEAR PHYS. 124, 49
AD71	41	PHYS.REV.C 3, 1808
AD71	101	BULL.AM.PHYS.SOC. 16, 829
AD72	6	PHYS.REV.C 5, 664
AD81	755	YAD.FIZ. 33, 1167
AG51	703	PHYS.REV. 84, 862
AH79	7	ANNALEN DER PHYSIK 36, 56
AJ54	1219	PHYS.REV. 95, 1531
AJ56	190	PHYS.REV. 103, 356
AJ59	93	PHYS.REV. 116, 1521
AJ59	100	BULL.AM.PHYS.SOC. 4, 258
AJ60	1211	PHYS.REV. 120, 500
AJ65	95	PHYS.REV.B 139, 592
AJ68	1223	NUCLEAR PHYS. 116, 481
AJ78	50	PHYS.REV.C 17, 1283
AL49	562	PHYS.REV. 76, 1430
AL50	680	PHYS.REV. 79, 227
AL50	698	PROC.ROY.SOC.(LONDON) 204, 500
AL51	524	PHYS.REV. 82, 786
AL52	505	PHYS.REV. 88, 425
AL52	526	PHYS.REV. 88, 433
AL54	92	PHYS.REV. 96, 684
AL54	881	CANADIAN J.OF PHYS. 32, 621
AL58	591	PHYS.REV. 111, 1129
AL59	1232	PHYS.REV. 114, 1040
AL60	109	PROC.PHYS.SOC. 75, 913
AL61	1134	PHYS.REV. 122, 862
AL61	2148	PROC.PHYS.SOC. 77, 234
AL63	741	BULL.AM.PHYS.SOC. 8, 538
AL65	126	NUCLEAR PHYS. 72, 436
AL66	91	PHYS.REV.C 143, 692
AL67	1039	YAD.FIZ. 6, 248
AL70	96	FIZIKA 2, 113
AL74	785	PHYS.REV.C 9, 787
AL76	857	NUOVO CIMENTO 36, 95
AL77	2020	NUCLEAR PHYS. 280, 61
AM49	1082	PHYS.REV. 76, 1421
AM57	196	PHYS.REV. 106, 775
AM58	193	PHYS.REV. 109, 1639
AM66	730	J.PHYSIQUE C 1, 62
AN60	312	NUCLEAR PHYS. 15, 464
AN62	1270	BULL.ACAD.SCI.USSR (PHYS.SER.) 26, 1147
AN63	356	NUCLEAR PHYS. 48, 299
AN63	1178	IZV.AKAD.NAUK SSSR (SER.FIZ.) 27, 1282
AN64	1135	PHYS.REV. 136,B 118
AN65	902	IZV.AKAD.NAUK SSSR (SER.FIZ.) 29, 211

1300 references contributed by LLNL and 230 added at Los Alamos. Several hundred additional references already located by LLNL and Group T-2 of Los Alamos will be added in the near future.

The utility codes are based on those written for ECSIL by D. E. Cullen.[42] Some have been updated to be CFT compatible, and some have been completely rewritten using the old programs as a guide. The following functions are currently operational:

DEX -- indexing code. Produces various sorted directory listings (see Tables V and VI).

CHK -- bibliographic checking code. Works with an index from DEX and the bibliography file to produce various bibliographic listings (see Figs. 3-5).

REF -- an interactive code for creating reference entries.

FIXDIR -- an interactive code for changing or inserting entries in an ECSIL2 directory.

FLTR -- reference filter code. Can be used to produce a complete bibliography for a particular author.

EDAD -- converts EDA data decks into ECSIL2 format.

UPD -- updates an ECSIL2 library (directory and data files) using input cards from EDAD or other sources.

These codes still need to be refined and extended. In addition, a code analogous to the ECSIL checking code ECSCEN is needed, and a code to convert from ECSIL to ECSIL2 will be required eventually.

This program is still in the early stages and suggestions from experimentors and evaluators are welcome.

C. ENDF-VI Development (R. E. MacFarlane)

During the last several years, we have been involved in a cooperative effort to design an enhanced format (the "ENDF-VI format") for the next version of the evaluated nuclear data libraries (the "ENDF/B-VI library"). The format will also be used for the Joint European File (JEF). A coordinated format proposal was submitted to the Cross Section Evaluation Working Group (CSEWG) in May, and a revised draft of the format manual was sent to the National Nuclear Data Center (NNDC) at Brookhaven in September. They are in the process of preparing a preliminary complete manual.

In the meantime, C. Dunford of the National Nuclear Data Center has prepared revised versions of the ENDF/B checking codes, and the following codes have been installed on the Los Alamos CDC 7600 environment using FTN5:

STANEF -- standardizes evaluations,

CHECKR -- checks for correct format,

FIZCON -- checks for valid data and conformance to recommended procedures, and

PSYCHE -- checks physics content.

A few minor changes were required to alter interactive input capabilities from a PDP10/VAX environment to the Los Alamos FTN/CFT environment.. In addition, a few minor errors were fixed, and a File 6 checking routine was added to PSYCHE. This routine checks Legendre distributions for negative emission probability and checks most reactions for energy-balance consistency.

The new ENDF checking codes were then used on the recent ^{63}Cu and ^{65}Cu evaluations from Hetrick, Fu, and Larson of the Oak Ridge National Laboratory (ORNL).[44] Several format errors were discovered and fixed.. In addition, the energy balance tests revealed two other problems.

First, there are errors as large as 20% in the energy balance for reactions like (n,2n), (n,n'p), and (n,p), especially near thresholds. These errors result from the relatively coarse energy bin structure (500 keV) used in the nuclear model calculations (see Ref. 44 for details). When spectrum of the emitted particle has an unfavorable shape, it is difficult to conserve cross section and average energy at the same time. This problem can be reduced by using smaller bins, variable-width bins, or special procedures for adjusting the model code output to fit energy production calculations. In practice, the new evaluations are an advance over ENDF/B-V, and the energy-balance errors observed should not distort the total nuclear heating and damage numbers significantly.

The second problem is with radiative capture. The ORNL evaluation did not address the region below 2 MeV, and the capture photon yield and spectra were simply carried over from ENDF/B-V. Unfortunately, the old evaluation has energy-balance errors up to 60% in the region from 100 keV to 1 MeV. We propose (with ORNL concordance) to reduce the yields to achieve explicit energy conservation. This should improve the results in the interim until ORNL completes their planned re-evaluation of copper at energies below 1 MeV.

III. NEUTRON ACTIVATION, FISSION PRODUCTS, AND ACTINIDES

A. Calculation of Neutron Sources and Activation in 50-MeV Proton Accelerator Materials (W. B. Wilson and E. D. Arthur)

Work is ongoing in Los Alamos Group AT-4 on the design of the Accelerator Test Stand Upgrade (ATSU) 50-MeV high-current $^{1}H^{-}$ linear accelerator, beam neutralizer, and facility. A major consideration in the facility design is the specification of radiation shielding for beam-spill and beam-dump neutrons and activation gamma rays. Recent thick-target neutron yield measurements for

30-MeV and 52-MeV protons on C, Fe, Cu and Pb by Nakamura et al.[45,46] have been used to describe the neutron source produced at the graphite beam dump and at ten positions/energies within the Cu of the drift tubes of the accelerator. These measured angular neutron yield spectra have been supplemented by calculations of angular neutron yield spectra for 5-50 MeV protons on Al and Cu. These calculations proceed as follows:

- Neutron-production cross sections and center-of-mass isotropic neutron spectra are calculated with the GNASH preequilibrium nuclear reaction model code[5] for each target nuclide on a grid of proton energies ranging from threshold to 50 MeV.

- Neutron-production cross sections and spectra are used with Kalbach-Mann angular distribution systematics[18] to produce double-differential neutron production cross sections.

- The neutron-production cross sections and double-differential neutron production cross sections are used with the proton stopping cross-section data of Anderson and Ziegler[47] to calculate the total thick-target neutron yield and the angular neutron yield spectra on a grid of laboratory proton energies and center-of-mass neutron energies and emission angles.

The GNASH calculated ^{63,65}Cu(p,x)n neutron-production cross sections, the proton stopping cross sections of Cu, and the calculated p+Cu thick target neutron yield are shown in Fig. 20. The calculated center-of-mass angular neutron yield spectrum for 30- and 50-MeV protons on Cu is shown in Fig. 21 at 30°; also shown is the corresponding measured laboratory system data of Nakamura et al.[46] for 30- and 52-MeV protons on Cu.

The thick target neutron yield and angular neutron yield spectra from protons on Al were also calculated, following the same procedure. The GNASH calculated ^{27}Al(p,X)n neutron-production cross section, the proton stopping cross sections of Al, and the calculated p+Al thick-target neutron yield are shown in Fig. 22. The calculated center-of-mass angular neutron yield spectrum for 30-and 50-MeV protons on Al is shown in Fig. 23 at 30°.

Calculations were also made to describe the radiation hazard associated with radionuclide production by beam spills in the copper of the accelerator's drift tubes. Activation of Cu was assumed to occur at each of ten locations in the linear system at ten corresponding proton energies. Thick target nuclide

production rates were calculated using evaluated p+Cu reaction cross sections and the proton stopping cross sections of Cu;[47] these production rates were used with basic radionuclide decay data, an assumed conservative one-year operating history, and a constant 0.3 μAmp/m spill rate to calculate the temporal radionuclide inventories and their aggregate gamma sources in a code utilizing CINDER methodology. The temporal sources were each isotropically transported without attentuation to representative response locations at which gamma fluxes were combined with response functions to calculate tissue dose equivalent rates. These rates, at positions 1 m offset from the accelerator axis at the exit of the accelerator, are shown in Fig. 23.

In an earlier work, Fulmer and Kindred[48] calculated activation and gamma dose-equivalent rates at 10 cm resulting from proton, dueteron, ^{3}He, and α bombardment of C, Al, Fe, Cu, and Ta. Data are presented for 10-65 MeV protons on Cu for irradiation times of 8-720 hours and cooling times of 1-168 hours. We have compared calculated dose equivalent rates from the present work (Los Alamos) and from Fulmer and Kindred[48] (Oak Ridge) in Table X for proton energies ≦ 50 MeV. In general, the agreement is poor for proton activation below 30 MeV. However, the agreement for incident 40- and 50-MeV proton activation is remarkably good considering that none of the data or calculational tools are common to the two calculations.

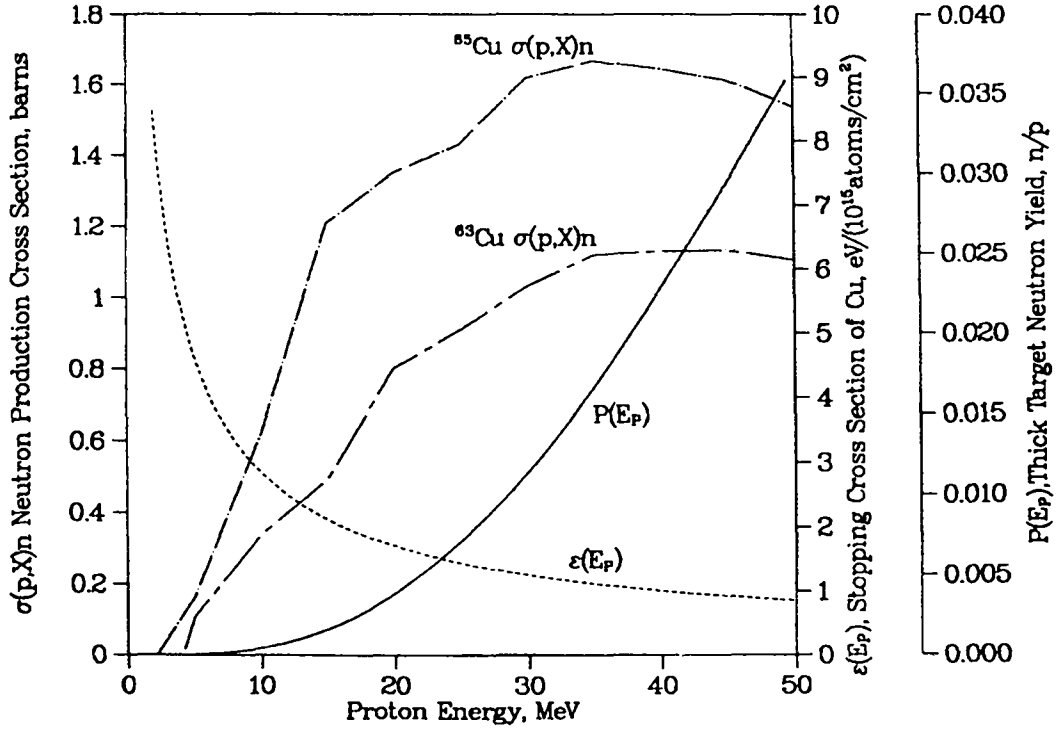

Fig. 20. GNASH-calculated $^{63,65}Cu(p,X)n$ cross sections, proton stopping cross section of Cu, and calculated p+Cu thick target neutron yield.

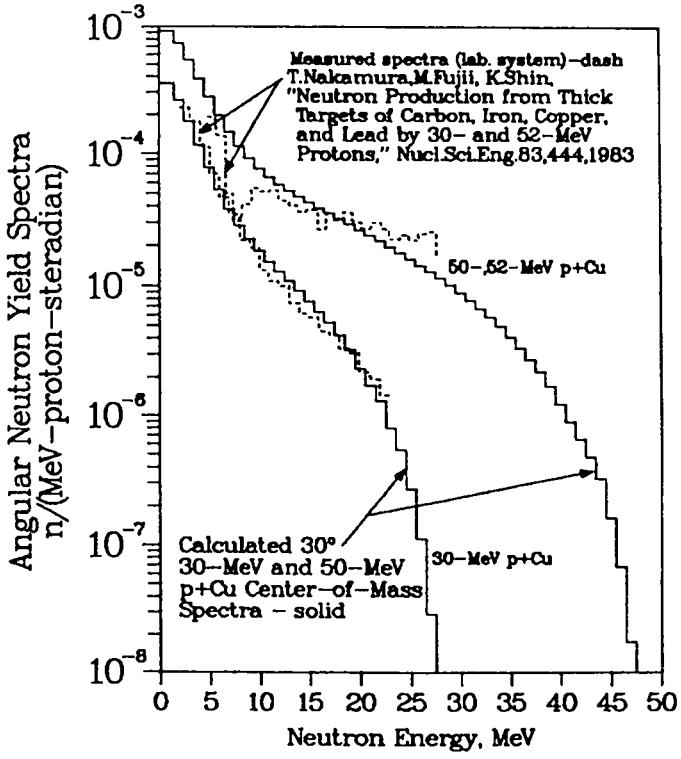

Fig. 21. Angular neutron yield spectra, p+Cu, 30°

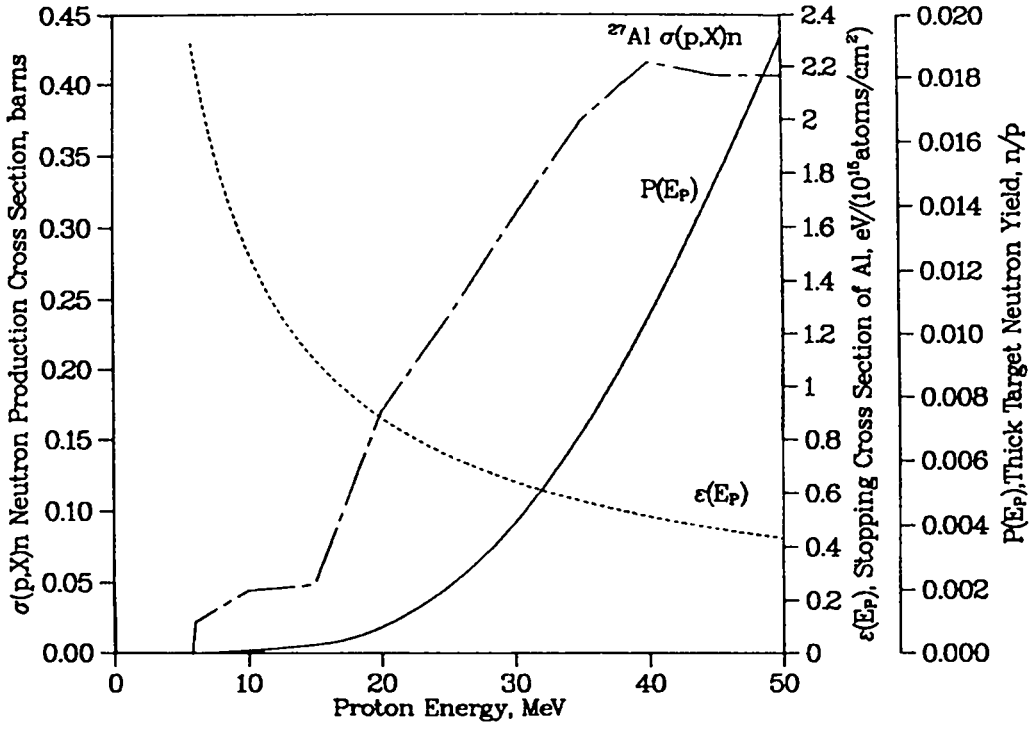

Fig. 22. GNASH-calculated ^{27}Al(p,X)n cross section, proton stopping cross section of Al, and calculated p+Al thick target neutron yield.

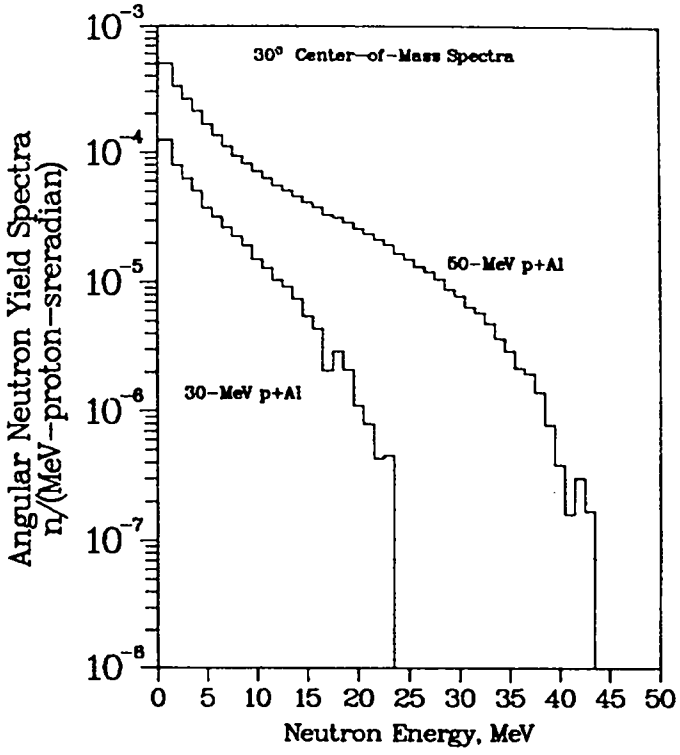

Fig. 23. Angular neutron yield spectra, p+Al, 30°.

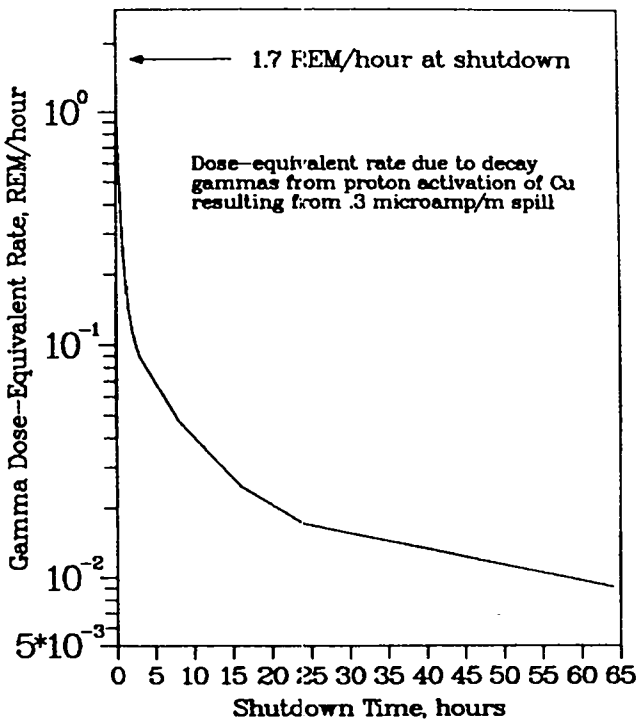

Fig. 24. Calculated dose-equivalent rate at beam exit 1 m from ATSU beam axis after a simulated 1-year, 40-hour/week 1% duty factor operation.

TABLE X

COMPARISON OF CALCULATED RADIATION DOSE RATE FROM THE DECAY OF ACTIVATION PRODUCTS PRODUCED BY PROTON IRRADIATION OF COPPER

BEAM TIME ,HRS	COOL TIME ,HRS	DOSE RATE AT 10 CM. (REM/HR-MICROAMP) 10-MEV PROTONS ORNL	10-MEV PROTONS LANL	20-MEV PROTONS ORNL	20-MEV PROTONS LANL	30-MEV PROTONS ORNL	30-MEV PROTONS LANL	40-MEV PROTONS ORNL	40-MEV PROTONS LANL	50-MEV PROTONS ORNL	50-MEV PROTONS LANL
8	1	.969	.106	5.18	.841	9.26	3.66	12.6	10.5	15.7	24.8
	8	.00059	.00167	.28	.161	2.12	1.47	3.19	3.06	4.04	4.42
	16	.00015	.00162	.153	.0873	1.12	.789	1.48	1.33	1.67	1.76
	24	.00015	.00162	.084	.0498	.61	.454	.764	.707	.832	.897
	168	.00015	.00159	.00045	.00475	.00050	.00575	.010	.006	.024	.007
24	1	.970	.109	5.58	1.07	12.3	5.74	16.8	14.5	20.8	30.3
	8	.00088	.00490	.517	.298	3.85	2.71	5.43	5.10	6.54	7.08
	16	.00045	.00485	.284	.167	2.07	1.51	2.66	2.46	2.96	3.18
	24	.00045	.00484	.157	.0981	1.13	.889	1.41	1.38	1.54	1.74
	168	.00044	.00476	.0013	.0142	.0015	.0170	.030	.019	.072	.021
48	1	.970	.114	5.73	1.16	13.3	6.58	18.1	15.8	22.3	31.9
	8	.0013	.00974	.604	.359	4.47	3.25	6.21	5.93	7.41	8.13
	16	.00089	.00968	.333	.207	2.41	1.85	3.10	2.98	3.47	3.85
	24	.00089	.00967	.184	.127	1.32	1.10	1.67	1.71	1.86	2.18
	168	.00087	.00951	.0027	.0284	.0029	.0335	.061	.037	.143	.041
168	1	.973	.138	5.77	1.25	13.5	6.92	18.5	16.3	22.9	32.6
	8	.0036	.0337	.664	.441	4.64	3.51	6.57	6.32	8.32	8.63
	16	.0032	.0337	.369	.285	2.50	2.06	3.35	3.27	3.95	4.22
	24	.0032	.0336	.207	.202	1.37	1.26	1.88	1.94	2.30	2.46
	168	.0031	.0331	.0092	.0988	.010	.144	.216	.125	.491	.135
720	1	.983	.244	5.80	1.57	13.6	7.28	19.2	16.7	24.5	33.0
	8	.0015	.140	.697	.758	4.68	3.87	7.28	6.71	9.60	9.05
	16	.0014	.140	.401	.601	2.54	2.41	4.07	3.66	5.56	4.64
	24	.0014	.139	.240	.519	1.41	1.63	2.59	2.33	3.90	2.89
	168	.0014	.137	.041	.410	.045	.470	.886	.511	2.00	.552

ORNL = C. B. Fulmer and G. Kindred, Oak Ridge National Laboratory (see Ref. 49).

LANL = Present work, Los Alamos National Laboratory.

B. Calculation of Neutron Sources in PWR Fuel [W. B. Wilson, R. T. Perry (Texas A&M University), J. E. Stewart (Q-1), and T. R. England]

The SOURCES code and library, under development for the past five years, calculates β^-,n-delayed, spontaneous-fission, and (α,n) neutron sources and spectra due to the decay of an input inventory of radionuclides in homogeneous media. Delayed neutron spectra are calculated with evaluated halflife and P_n data using preprocessed spectra for the 105 individual precursors. Spontaneous-fission spectra are calculated with evaluated halflife, SF branching, and $\bar{\nu}$ data using Watt spectrum parameters for 43 actinides. The (α,n) spectra are calculated with a library of nuclide decay α spectra, evaluated (α,n) cross-sections and product-nuclide level branching fractions, and functional α stopping cross sections using an assumed isotropic neutron angular distribution in the center-of-mass system.

These neutron spectra are now supplemented by photoneutron spectra calculated with PHONX84, an evolved version of PHONEX. PHONX84 uses an input γ energy-binned fluence and deuterium atom density, and evaluated $^{2}H(\gamma,n)$ photoelectric and photomagnetic cross sections using isotropic photomagnetic and $\sin^{2}\theta$ photoelectric neutron angular distributions in the center-of-mass system. Individual γ spectra for 86 fission-product nuclides have been processed from ENDF/B-V. Monte Carlo photon transport calculations have been made with MCNP for γ sources homogeneously distributed in the fuel of a ZR-4 clad PWR fuel rod centered in a repeating cubic cell with reflecting boundaries and outside dimensions equal to the rod pitch; these calculations yielded water-volume integrated γ energy-binned fluences for unit γ sources at each energy boundary of the ¼-MeV bin structure extending to 7 MeV. PHONX84 calculations of photoneutron spectra were performed for unit fluences in each γ energy bin. The unit-source fluences were then combined with the unit-fluence photoneutron spectra and the processed ENDF/B-V fission-product γ spectra to produce unit-decay PWR photoneutron spectra for each fission-product nuclide.

The combined SOURCES/PHONX84 capability has been demonstrated in the calculation of the neutron source in discharged 31.5-GWd/tU 2.56% initial enrichment H. B. Robinson-II PWR fuel for cooling times extending to 100 years. The inventory of fission products and actinides at shutdown and at cooling times of interest were obtained in CINDER calculations. These calculated inventories were input to SOURCES for the β^{-},n-delayed, spontaneous-fission and (α,n) source and spectra contributions; photoneutron contributions were obtained by combining the inventories with the unit-decay photoneutron spectra described above. The total neutron source rates associated with each source are shown in Fig. 25 for shutdown times extending to 100 y. Neutron source spectra have also been calculated in a 100-keV bin structure; the neutron spectra calculated at a shutdown time of 700 s are shown in Fig. 26.

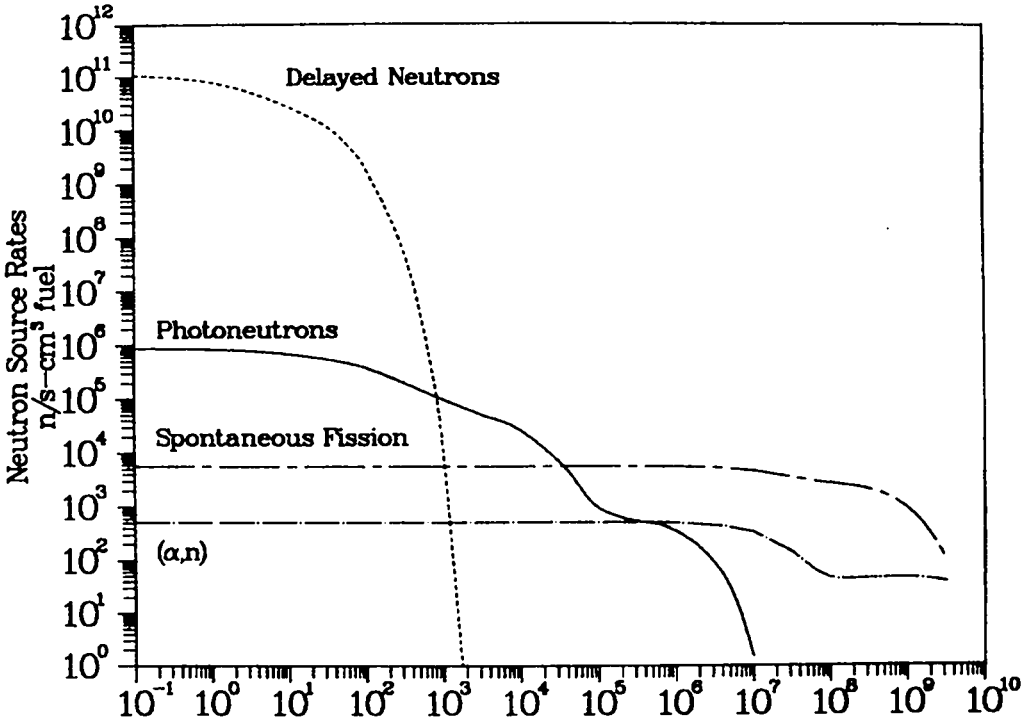

Fig. 25. Calculated neutron sources in 31.5 GWd/tU 2.56% H. B. Robinson-II PWR fuel, 700 s following shutdown.

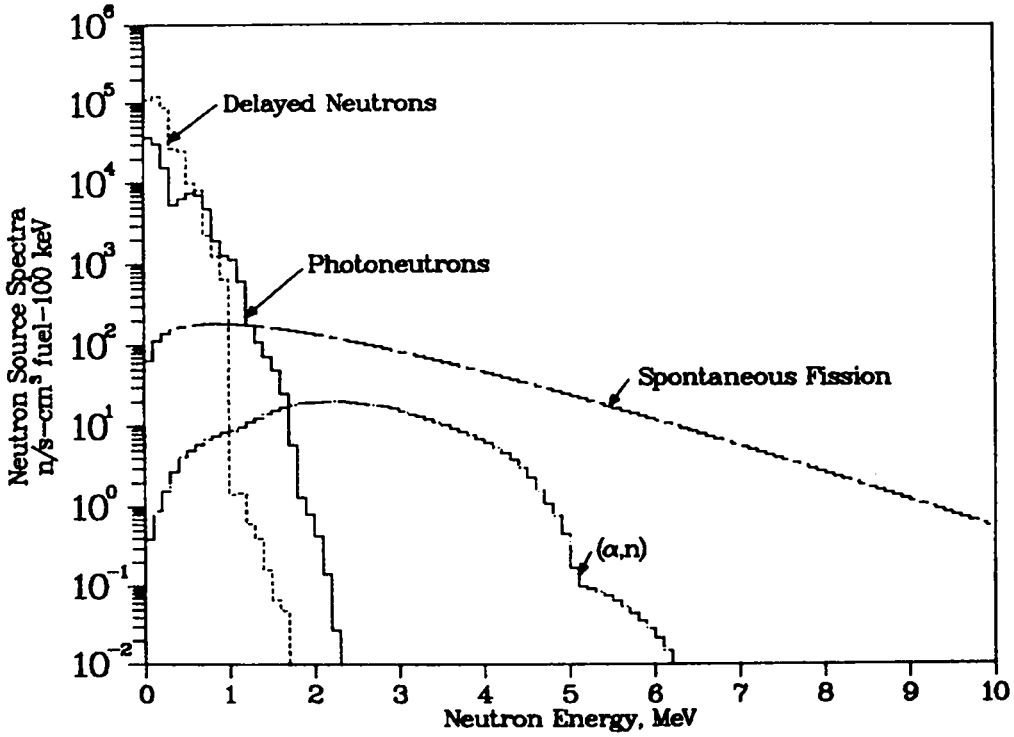

Fig. 26. Calculated neutron source spectra, 31.5 GWd/tU 2.56% H. B. Robinson-II PWR fuel, 700 s following shutdown.

C. Application of Evaluated Fission-Product Delayed-Neutron Precursor Data in Reactor Kinetics Calculations [R. T. Perry (Texas A&M Univ.), W. B. Wilson, T. R. England, and M. C. Brady (Texas A&M Univ.)]

The temporal production of β^-,n-delayed neutrons following fission have routinely been described using six precursor groups. These groups originated as fits to experimentally measured neutron signals following fission pulses or long irradiations in critical assemblies.[49] Use of the six-group delayed-neutron representation in reactor kinetics calculations has become an industry standard.

Six-group data, describing the aggregate temporal delayed-neutron behavior, have been progressively reevaluated for versions of ENDF/B.[50] Data describing the individual precursors have been produced in more recent measurements and nuclear model code calculations. The fission-product decay data and fission yields of ENDF/B-V and the updated precursor decay data of Ref. 51 form a consistent set of delayed-neutron precursor data with which a variety of delayed-neutron properties may be calculated.

This data set includes the identities, decay constants, neutron branching (P_n) values, detailed neutron emission spectra, and fission yields of 105 delayed-neutron precursors. Each of these are yielded directly in fission; all but one are also produced by the decay of one or more parent nuclide. The description of the temporal inventory and delayed-neutron production rate of the 105 precursors requires the description of the temporal inventory of 121 additional parent radionuclides.

We have used this detailed library of data to describe the temporal concentrations of the 226 fission-product nuclides, including the 105 delayed-neutron precursors, and their individual and aggregate delayed neutron contributions in point reactor kinetics calculations. In order to account for the production of delayed-neutron precursors by the decay of parent nuclides, the kinetics equations have to be reformulated. The equations become:

$$\frac{dn(t)}{dt} = \frac{\rho(t)-\beta}{\Lambda} n(t) + \sum_{i=1}^{226} \lambda_i P_n^i N_i(t)$$

$$\frac{dN_i(t)}{dt} = \frac{y_i}{\bar{\nu}\Lambda} n(t) - \lambda_i N_i(t) + \sum_{j=1}^{226} \lambda_j B_{j\rightarrow i} N_j(t) \ ,$$

where n(t) is the neutron density as a function of time, t; $\rho(t)$ is the reactivity, Λ is the prompt neutron generation time, β is the delayed neutron fraction; $N_i(t)$ is the temporal concentration of fission-product nuclide i; λ_i is the decay constant of nuclide i; y_i is the independent fission yield of nuclide i; $\bar{\nu}$ is the average number of neutrons per fission; P_n^i is the branching fraction for producing a neutron from the decay of nuclide i; and $B_{j\rightarrow i}$ is the nuclide j decay branching fraction for production of nuclide i.

With the exception of the term $\sum_{j=1}^{226} \lambda_j B_{n\rightarrow i} N_j(t)$, the equations are similar in form to the point reactor kinetics equations. Thus, the numerical methods used in the AIREK-3[52] code, with some modifications to handle the extra term, are applied to obtain solutions for $N_i(t)$ and n(t), as functions of time.

Several methods were used to validate the numerical solution of the revised code, now called AIREK-10. The validations included:

1. Comparison with an analytical solution of neutron density 10 seconds following a step input of reactivity. The comparison was made with a fictitious set of nuclide data, small enough that an exact solution could be obtained.

2. Comparison with aggregate delayed neutron production rates calculated by CINDER-10 following pulse and infinite irradiation.

In all cases, excellent agreement was obtained.

Calculations of the neutron density as a function of time were made using six group constants and compared with the results using 226 nuclides.

In Table XI, the neutron density at 9.98 seconds following a + \$0.50-step input in a ^{235}U thermal fission system for various six group parameter sets and 105 precursor/226 nuclide parameters is given.

TABLE XI

NEUTRON DENSITY 9.98 s FOLLOWING A +\$0.50 STEP, ^{235}U THERMAL FISSION

105-precursor 226-nuclides	England[52] 6-groups	Keepin[50] 6-groups	ENDF/B-V[51] 6-groups
16.167	13.783	12.147	11.892

The significant result of this comparison is that the neutron density following the step input, calculated with the evaluated precursor data, is significantly greater than that calculated with any of the 6-group approximations.

The implication is that reactivity measurements evaluated with 6-group calculations may significantly underestimate control rod worths and all reactivity worths evaluated relative to control rod positions (e.g., temperature, void, xenon, and excess reactivity worths).

Initial calculations have been limited to ^{235}U thermal systems; calculations for other systems and inclusion of neutron spectral effects are proposed.

D. Evaluation of Experimental Delayed Neutron Spectra [T. R. England, M. C. Brady (Texas A & M University)]

Experimental delayed neutron spectra were received from K. L. Kratz (Institut für Kernchemie der Universität Mainz, Mainz, Germany) in November 1983. Spectral data were included for ^{87}Br, ^{89}Br, ^{90}Br, ^{91}Br, ^{92}Br, ^{92}Rb, ^{94}Rb, ^{96}Rb, ^{97}Rb, and ^{98}Rb. The data were in the form of counts per channel vs channel number and a value of 4 keV/channel was given to calibrate a relative energy scale.

All spectra have been converted to energy scales. The spectra for ^{87}Br, ^{92}Rb, and ^{94}Rb have been normalized and reduced to 10 keV-energy bins, and average energies have been calculated. The energy scales for these three isotopes are estimated to be accurate to ±4 keV. The energy scales for the remaining bromine isotopes should be improved to similar accuracy when corrections are made to subtract the thermal peak present in each of these spectra ($^{89-92}Br$). Slight corrections are also required for the energy scales of ^{96}Rb and ^{98}Rb. The spectrum for ^{97}Rb appears to contain a background of counts, which must be removed, and requires a slight correction in its energy scale to achieve an accuracy of ±4 keV. Finally, these remaining spectra will be normalized and reduced to 10 keV bins and average energies will be calculated.

These data are reduced to 10 keV bins because most of our measured data from other sources and all model estimated spectra is in 10-keV bins.

We are, however, lacking an adequate method of determining the uncertainties associated with the peaks. This is primarily due to a lack of information pertaining to the unfolding procedure used to convert the data from pulse height spectra to delayed neutron spectra. We have contacted K. L. Kratz and hope to resolve the problem.

Figures 27 and 28 provide comparisons of earlier data received from Gösta Rudstam (Swedish Research Councils Laboratory, Nyköping, Sweden) with the current Kratz data for ^{87}Br and ^{94}Rb, respectively.

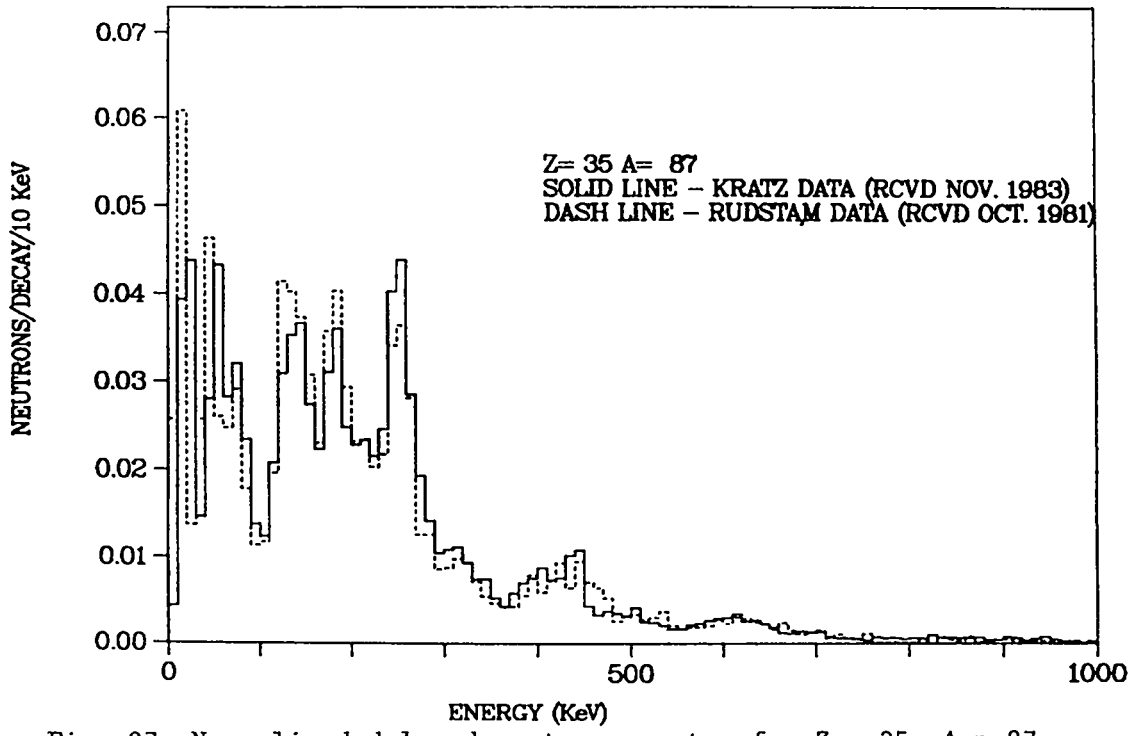

Fig. 27. Normalized delayed neutron spectra for Z = 35, A = 87.

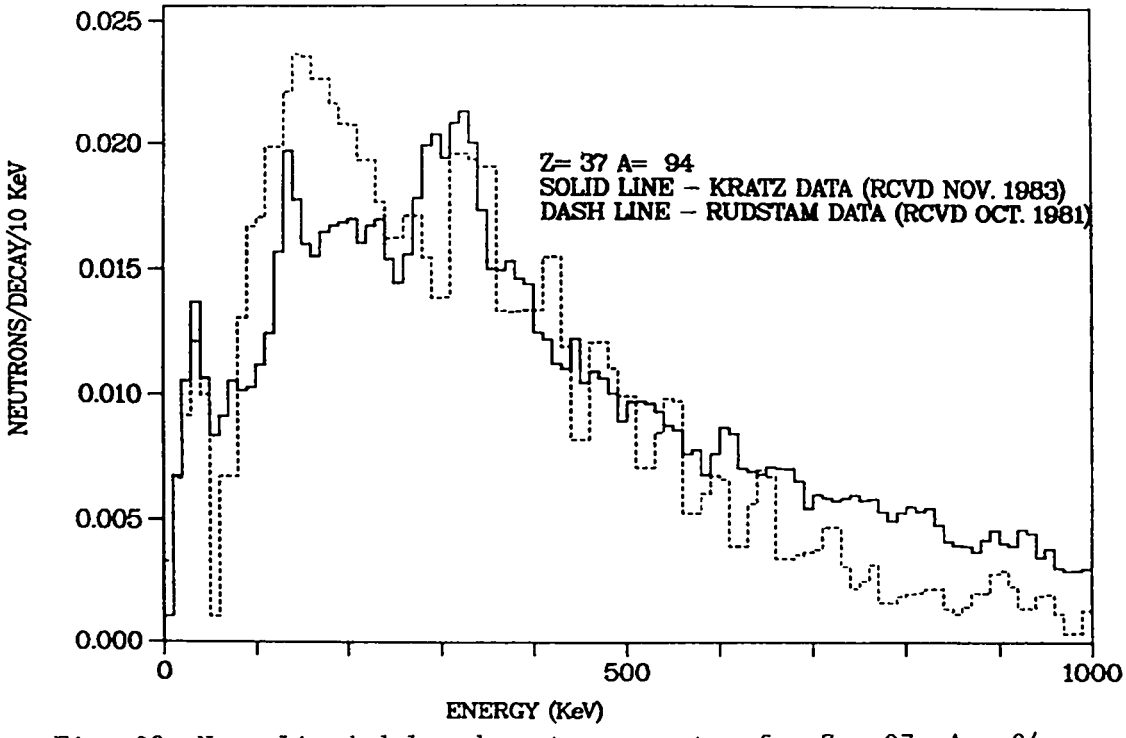

Fig. 28. Normalized delayed neutron spectra for Z = 37, A = 94.

E. Feasilibity Study of a Thermal Neutron Driven 14-MeV Neutron Source [R. T. Perry, T. A. Parish (Texas A&M University), W. B. Wilson]

The purpose of the study was to determine the feasibility of using a flat plate containing ^{6}LiD in conjunction with a University Research Reactor to produce a simulated fusion plasma neutron source. The fusion plate would have possible use in benchmarking theoretical calculations of importance in fusion reactor design.

It has been well established[53] that fusion neutrons can be produced through a series of nuclear transformations, beginning with a thermal neutron capture in ^{6}Li:

$$n + {}^{6}Li \rightarrow t + \alpha + Q \quad . \tag{1}$$

If the ^{6}Li is in the form of ^{6}LiD, then the triton produced in Eq. (1) is sufficiently energetic (2.73 MeV) to produce a fusion neutron from the d-t reaction:

$$d + t \rightarrow \alpha + n + Q \quad . \tag{2}$$

The 1MW TRIGA Research Reactor at Texas A&M University's Nuclear Science Center has facilities large enough to handle a plate containing ^{6}LiD of dimensions 60 x 60 cm. The average thermal flux across the face of the fusion plate would be 2×10^{12} n/cm^2 - s. The neutron source strength and spectra from this fusion plate were determined in this study.

A 324-gram ^{6}LiD plate measuring 60 x 60 cm x 1 mm has been selected. The 1-mm thick sheet of ^{6}LiD will capture 99% of the thermal neutrons entering. By computing the variation of the thermal flux inside the slab and using the range of a 2.7-MeV triton in ^{6}LiD, it was calculated that between 10 and 30% of the the tritons produced will escape a 1-mm thick slab of ^{6}LiD. These two values are based, respectively, on whether the thermal flux is assumed to be a beam or isotropic on the face of the slab. The ^{6}LiD could be thinner than 1 mm and still capture most of the incident neutrons; however, the triton loss would become excessive.

As noted earlier, the triton produced in Eq. (1) may result in the d-t reaction. While this is the principle reaction, the production of neutrons from the t-^{6}Li reaction must also be considered.

The neutron yields for these two reactions were calculated using the thick target approximation with methodology developed earlier.[54] Stopping powers used were those of Anderson and Ziegler.[47] Neutron production cross sections for ^{6}Li were obtained from a paper by A. K. Val'mer, et al.[55] Linear interpolation was used to obtain the cross section over the energy range of interest; thus, considerable error could be present, particularly at high energies. The neutron range in LiD was computed from the stopping power relationship to be 90 μm. The d-t cross sections were obtained from Miley, et al.[56]

The results of the thick-target neutron yield calculations for a 2.73-MeV triton in ^{6}LiD are 180 neutrons from d-t reactions and 107 neutrons from t-^{6}Li reactions per 10^{6} tritons produced. These values compare favorably with earlier calculations;[57] however, they compare poorly with experimental values reported in the literature.[57,58] This discrepancy is probably due to a combination of difficulties in accurately measuring the high energy flux, the escape of tritons from the sample, and errors in the basic interaction data.

The total neutron production for the 60 x 60-cm device driven by the 1-MW reactor would be 9.6×10^{11} n/s of neutrons from the d-t reaction. From the T-^{6}Li reaction, the device would produce 5.8×10^{11} n/s.

The spectra were calculated assuming isotropic neutron production in the center-of-mass system,[59] which results in uniform energy distribution over possible energy ranges in the laboratory system. In reality, neutrons are produced anisotropically in both the d-t and t-^{6}Li reactions. We note, however, that the d-t reaction is dominant and the majority of these neutrons are produced at low triton energies where little anisotropy is expected. Thus, we felt that the spectra produced with this assumption would be adequate and more detailed calculations were not needed at this time.

A second assumption made in calculating the spectra was that the product nucleus would be produced in the ground state. This is well founded for the dominant d-t reaction, because the product nucleus, He^{4}, has its first energy level at 20.1 MeV and this level could be populated only as a result of d-t reactions induced by triton of almost maximum energy (2.73 MeV).

For the t-^{6}Li reaction, it is possible to populate various energy levels of the product nucleus, ^{8}Be, thus conflicting with the above ground-state assumption. (See contribution by Hale, George, and Lisowski, p. 1 of this progress report.) However, if neutrons are produced by a reaction in which the product nucleus remains in an excited state, the emitted neutron would receive

a lower energy than if the residual nucleus were in the ground state. Therefore, the high energy portion of the neutron spectrum would be dominated even more by the d-t reaction. As simulation of a fusion reactor is the desired goal, it is felt that, if the spectra produced by these calculations are adequate to meet design goals, then the actual spectra produced would certainly be adequate as well, our calculations being on the conservative side. In addition, work is currently in progress[60] to produce a more accurate T-^{6}Li spectra that will be incorporated in our work.

The spectrum, a composite of d-t and t-^{6}Li reactions, weighted by the respective neutron yields, is shown in Fig. 29. Note that the spectrum plotted in the figure is actually a histogram, normalized to 1, over 0.1 MeV intervals, and each bar represents the fraction of the total neutrons contained in that energy interval. The small intervals for the histogram give the appearance of a continuous function.

The total neutron source strength is probably adequate for fusion neutron blanket experiments, for code development, and for methods benchmarking. The spectrum, dominated by the d-t reaction, reasonably represents a d-t fusion neutron spectrum corresponding to a plasma temperature of about 400 keV.

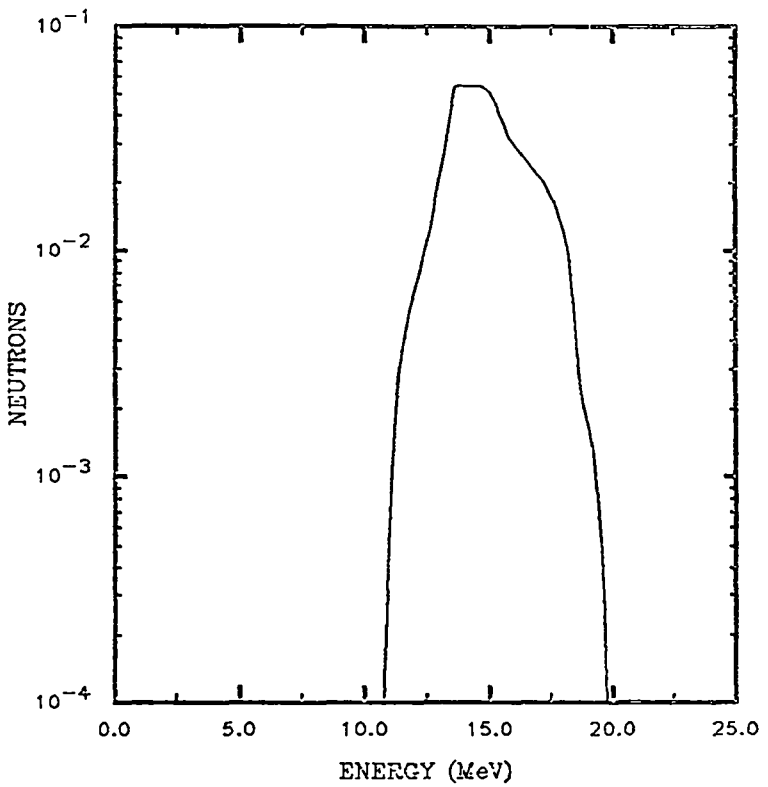

Fig. 29. Neutron spectra for (t,n) reactions in ^{6}LiD.

Calculations for LCCEWG-5: FFTF Cycle 1 Depletion* (R. J. LaBauve, D. C. George, T. R. England, W. B. Wilson, and R. E. MacFarlane)

Calculations for the FFTF, Cycle 1 (A and B) depletion part of LCCEWG Benchmark #5[61] were run using the DANDE code system[62] illustrated in Fig. 30. As was done for our calculations for the FFTF High Power Characterizer experiment (HPC) part of LCCEWG-5,[63] the TRANSX code[64] was used in the data processing module to generate the ISOTXS file, the DIF3D code[65] was used for core neutronic calculations, and the CINDER-3 code[66] for depletion. The basic nuclear data used as input to TRANSX and CINDER-3 were from ENDF/B-V[67] processed by the NJOY code[68] into 80- and 154-group fine-group libraries, respectively. (Note that the Revision-2 evaluation for ^{239}Pu is not included in these fine-group libraries.) The weighting spectra used in the TRANSX and CINDER-3 codes for collapsing to 12 groups were those from the two-dimensional R-Z HPC model as calculated with the DIF3D diffusion code. Details are given in Ref. 63.

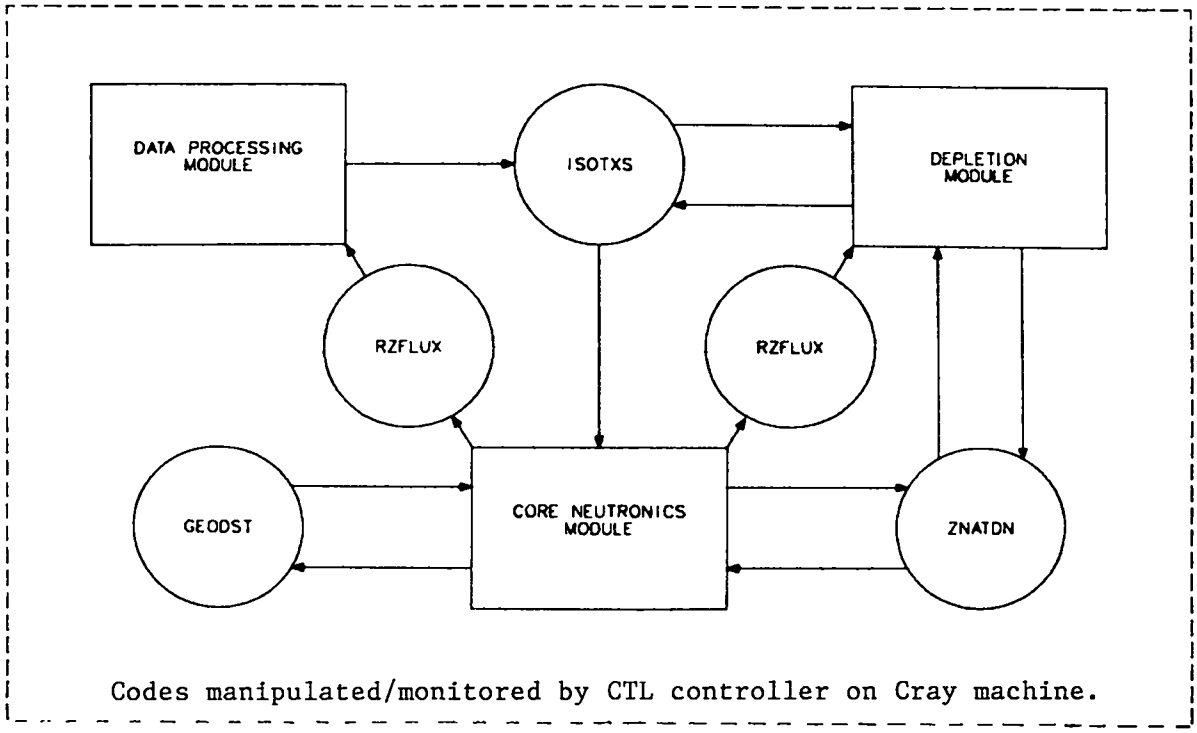

Fig. 30. DANDE code system for reactor core analysis.

*LCCEWG-5 (Large Core Code Evaluation Working Group-Problem 5); see Ref. 61.
FFTF (Fast Fission Test Facility)

The nodal, three-dimensional hexagonal-Z option of the DIF3D code was used for the principal core neutronics calculations. The prime advantage of using the nodal option is in gaining relatively good accuracy for short computing times. The DIF3D calculational time used in a single depletion step was about four minutes on the CRAY computer. The disadvantage of the nodal option, however, is that considerable spatial resolution is lost. In our FFTF model, described below, a hexagon contains only a single "x-y" mesh point, in contrast to a triangular-Z finite-difference problem in which a hexagon contains a minimum of six mesh points. Consequently, our calculational results were restricted to region averages.

Comparison two-dimensional depletion calculations were also run in which the nodal hexagonal option was specified in the DIF3D code. Comparison two-dimensional transport depletion calculations were begun, using the TWOHEX code,[69] but due to time/funding limitations, these could not be completed. Running times for the two-dimensional core neutronics module were about twenty seconds for the diffusion and three minutes for the transport calculations.

The input configuration for CINDER-3 was essentially the same as that used in the HPC calculations with the exception of the occurrence of different fuel assemblies having differing exposure histories, thereby requiring the designation of more regions. As a result, a single depletion time-step required about 15 seconds on the CRAY computer.

To obtain a starting model for FFTF Cycle-1A depletion (BOC-1A), a six-time step DANDE run was made to estimate explicit nuclide, fission-product lump, and individual fission-product densities. The explicit-nuclide and aggregate fission-product lump densities were transferred between the core neutronics and depletion modules via ZNATDN, the standard file[70] for explicit nuclide densities; the individual nonexplicit-nuclide chain densities, however, remained in the depletion module and were updated in each time step.

The six time steps used in the approach to BOC-1A were selected mainly from Fig. 6 of the benchmark specifications[61] and included irradiation times of 10, 15, 19, 24, and 32.4 full-power days, followed by a shutdown time of 120 days, which was estimated from Table I of the benchmark specifications. Note that Assembly #2607 (Fig. 6 of the benchmark specifications) that actually received 23.6 full power days was assumed to have received 24.

The exposure scheme used in the approach to BOC-1A is outlined in Table XII. The exposure each assembly received is indicated by a letter of the alphabet, with the exception of those receiving 32.4 full-power days to which no letter is assigned. Otherwise, those with a final letter "A" received 24 days; those with "B," 19 days; those with "C," 15 days; those with "D," 10 days; and those with "E," 0 days. The compositions of all other regions, above and below core, were as specified for the HPC calculations (Ref. 63). Note that for this part of the calculation, no replacement or change in position was made for any of the assemblies, as indicated in Table A-1 of the benchmark specifications; thus, each remained in the same position during the entire calculation for the approach to the conditions of BOC-1A. The control assembly bank was, however, positioned as indicated on p. 10 of the benchmark specifications. The reference k_{eff} at the end of this series of calculations was 0.98358. Details are shown in Table XIII.

Results for the Cycle 1 diffusion, three-dimensional depletion calculations (DIF3D in the core calculational module of DANDE) are shown in Table XIV. Cycle 1A was run in two time steps, 17 and 17.1 days, respectively, and Cycle 1B was run in four 16.95-day time steps. A shutdown period of 94 days was assumed between EOC-1A and BOC-1B. The control assembly bank was proportionately withdrawn for intermediate time steps. The reactivity gain between sub-cycles was the sum of 0.0005 in k_{eff} for the 94-day cooling time and 0.0013 for the additional 1.3-cm control rod bank withdrawal. The final k_{eff} of 0.98353 for EOC-1B compared with 0.98358 for BOC-1A indicates the calculated reactivity loss/control bank worth to be essentially "in balance." The discrepancy amounts to only about 0.02¢/full-power day.

For comparison purposes, a series of two-dimensional depletion calculations was run for Cycles 1A and 1B. Core mid-plane geometry and nuclide densities were used in the two-dimensional model, and the "extrapolation distance" of the DIF3D card type 12 for representing buckling was varied to give a k_{eff} approximately equal that for the three-dimensional BOC 1-A model. The resulting buckling was $4.395 \times 10^{-4}/cm^2$. Note that, as the beginning time for Cycle-1 was taken as zero for the two-dimensional runs, the individual nuclide chains in the depletion module were all initialized; whereas the first CINDER-3 run for the three-dimensional problems was a continuation of the approach to Cycle-1 depletion. All explicit nuclide densities, including those for the fission product burnup, however, were taken from the three-dimensional BOC-1A problem.

TABLE XII

DESIGNATIONS OF CORE REGIONS FOR LCCEWG-5 FFTF CYCLE-1 MODEL

Region Number	Region Name	Zone Number	Assembly Type	Exposure (days)
1	ASF	1	Axial Shield-Fuel	-
2	ARF	2	Axial Reflector-Fuel	-
3	INF	3	Insulator-Fuel	-
4	F32C	21	DFA-3.2	15.0
5	GPF	5	Gas Plenum-Fuel	-
6	F32	17	DFA-3.2	32.4
7	ICS	15	ICSA	-
8	CRS	4	Control Assembly Shield	-
9	NAC	6	S.R. Na Channel	-
10	BPC	7	Below Poison Channel	-
11	ABC	8	C.R. Absorber	-
12	APC	16	Above Poison Channel	-
13	DE2B	19	DE1-2	19.0
14	F42E	33	DFA-4.2	0.0
15	F32B	20	DFA-3.2	19.0
16	DE1R	18	DE1-1R	32.4
17	F32D	22	DFA-3.2	10.0
18	F42B	32	DFA-4.2	19.0
19	F42	30	DFA-4.2	32.4
20	F31	23	CFA-3.1	32.4
21	DRL	9	Driveline-Control Assembly	-
22	SRB	31	SRF-1 and 2	19.0
23	F31A	28	CFA-3.1	24.0(23.6)
24	F41B	31	CFA-4.1	19.0
25	F31B	29	DFA-3.1	19.0
26	DE5	26	DE1-5	32.4
27	DE6	27	DE1-6	32.4
28	DE3B	24	DE1-3	19.0
29	VOT	35	VOTA	-
30	HA6	37	HA006	-
31	W42B	39	WB042	19.0
32	DE4	25	DE1-4	32.4
33	F41E	34	CFA-4.1	0.0
34	LRS	10	Lower Radial Shield	-
35	RR1	11	Radial Reflector #1	-
36	URS	13	Upper Radial Shield	-
37	HA3	36	HA003	-
38	W18B	38	WB018	19.0
39	RR2	12	Radial Reflector #2	-
40	USNA	14	50% Upper Shield, 50% Na	-

TABLE XIII

APPROACH TO CYCLE-1A

Exposure Time (Days)	Cooling Time (Days)	Rod Position (cm Withdrawn)	K-effective
0.0	0.0	49.3	0.99898
8.4	0.0	43.2	0.99056
5.0	0.0	43.2	0.98964
4.0	0.0	43.2	0.98844
5.0	0.0	43.9	0.98768
10.0	0.0	42.6	0.98335
0.0	120.0	42.6	0.98358

TABLE XIV

CYCLE-1 RESULTS 3-DIMENSIONAL CALCULATIONS

Total Exposure (days)	Cooling Time (Days)	Rod Position (cm Withdrawn)	K-eff	Comment
0.0	0.0	42.6	0.98358	BOC-1A
34.1	0.0	53.0	0.98344	EOC-1A
34.1	94.0	54.4	0.98527	BOC-1B
101.9	0.0	81.3	0.98353	EOC-1B

The two-dimensional depletion results are shown in Table XV. Note that the reactivity loss for the first time step shown in the table is less than the average. As indicated above, this is due to the fact that depletion, i.e., density changes for the chain nuclides before Cycle 1, was not accounted for in the CINDER chain structure for the two-dimensional runs. On the other hand, the cooling time between Cycles 1A and 2B causes a somewhat larger than average value for reactivity loss to be given for the first time step in Cycle 1B. The overall Cycle 1 reactivity loss of 10.1¢/full-power day for the two-dimensional calculations is about 6% lower than the 10.7¢/full-power day calculated for the HPC experiment in three-dimensions (see Ref. 63).

The two-dimensional reactivity loss is consistent with calculated control rod withdrawal distance, however. Figure 31 shows the worth of the control assembly bank as calculated using the 1/3-core HPC model described in Ref. 63.

TABLE XV

CYCLE-1 DEPLETIONS 2-DIMENSIONAL RESULTS

Total Exposure (days)	Cooling Time (days)	K-eff	Reactivity Loss (Cents/FPD)
0.0	0.0	0.98355	
			9.3
17.0	0.0	0.97853	
			10.2
34.0	0.0	0.97296	
			--
34.0	94.0	0.97350	
			11.5
51.05	0.0	0.96729	
			10.2
68.0	0.0	0.96181	
			10.1
84.95	0.0	0.95636	
			10.2
101.0	0.0	0.05092	
		Cycle-1 Reactivity Loss	10.1

Note: β_{eff} = 0.00318 used in cents/FPD calculations.

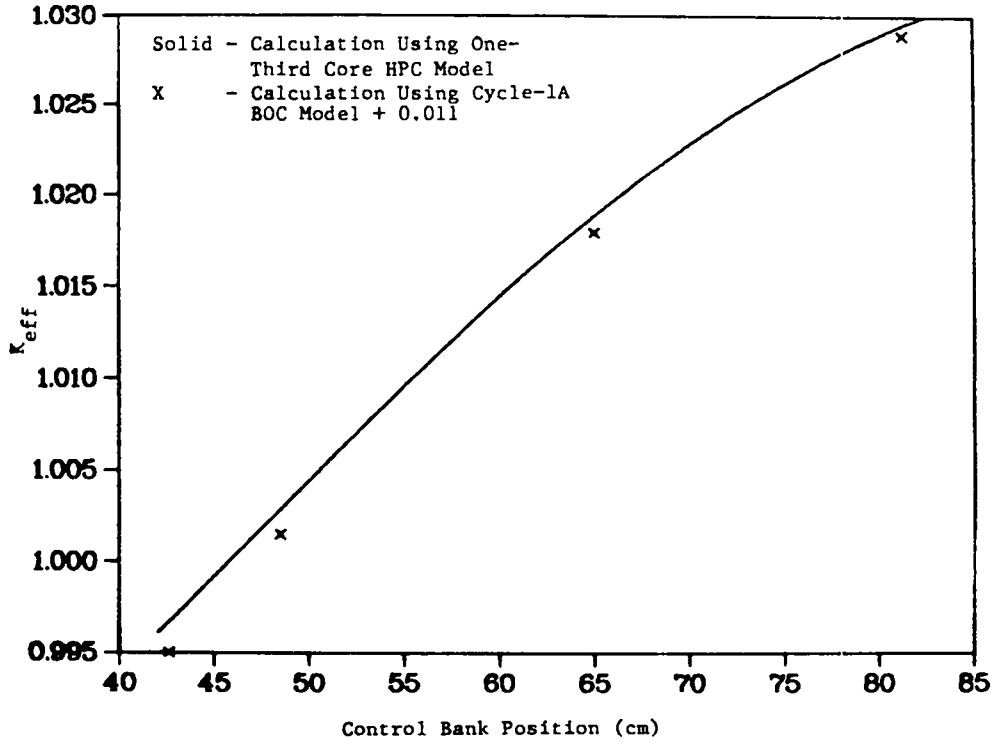

Fig. 31. FFTF control bank worth (no depletion).

(A few calculated points are shown using the BOC-1A full core model for comparison.) Reading a k_{eff} value of 0.99670 from the graph for a rod position of 42.6 cm, the initial withdrawn position for Cycle 1, and adding the two-dimensional calculated reactivity loss of 0.03263 for Cycle 1 results in a graph value of 1.02933 for k_{eff}. This is equivalent to a rod withdrawn position of 81.0 cm, which compares favorably with the experimental 81.3 number given in the benchmark specifications.

Two-dimensional transport depletion calculations using the TWOHEX code were begun, but time/funding limitations did not permit completion. The first run of the series, BOC-1A, using the two-dimensional DIF3D buckling gave a k_{eff} of 0.99201, indicating a transport/diffusion "correction" of 0.0086 $\Delta k/k$.

REFERENCES

1. P. W. Lisowski, R. E. Brown, J. C. Gursky, S. D. Howe, N. Jarmie, and G. L. Morgan, "Cross Sections for the $^{6}Li(t,n)2\alpha$ Reaction," Bull. Am. Phys. Soc. 29, 748 (1984).

2. A. J. Elwyn, R. E. Holland, C. N. Davids, J. E. Monahan, F. P. Mooring, and W. Ray, Jr., "Cross Sections for the $^{6}Li(^{3}He,p)$ Reaction at Energies Below 2 MeV," Phys. Rev. C 22, 1406 (1980).

3. P. G. Young and L. Stewart, "Control Materials and Light Coolant Cross-Section Data," Prog. Nucl. En. 13, 193 (1984).

4. E. D. Arthur, Comp., "Applied Nuclear Data Research and Development Semiannual Progress Report: April 1-September 30, 1983," Los Alamos National Laboratory report LA-10069-PR (June 1984).

5. P. G. Young and E. D. Arthur, "GNASH: A Preequilibrium-Statistical Nuclear Model Code for Calculations of Cross Sections and Emission Spectra," Los Alamos Scientific Laboratory report LA-6947 (November 1977).

6. P. G. Young, G. M. Hale, and D. R. Harris, "Annual Progress Report of the Defense Nuclear Agency Sponsored Cross-Section Evaluation Group at Los Alamos Scientific Laboratory: July 1, 1973 through June 20, 1974," Los Alamos Scientific Laboratory report LA-5759-PR (1974), p. 5.

7. V. J. Orphan. N. C. Rasmussen, and T. L. Harper, "Line and Continuum Gamma-Ray Yields from Thermal-Neutron Capture in 75 Elements," Gulf General Atomic report GA-10248 (1970).

8. R. J. Howerton and E. F. Plechaty, "A Formalism for Calculation of Neutron Induced Gamma-Ray Producion Cross Sections and Spectra," Nucl. Sci. Eng. 32, 178 (1968).

9. P. G. Young, "Nuclear Model Code Calculations for n + ^{93}Nb Reactions," in Los Alamos T-2 Internal report T-2-IR-83-4 (1983), p. 6.

10. E. D. Arthur, P. G. Young, D. G. Madland, and R. E. MacFarlane, "Evaluation and Testing of n + ^{239}Pu Nuclear Data for Revision 2 of ENDF/B-V," Nucl. Sci. Eng. 88, 56 (1984).

11. B. A. Magurno and P. G. Young, "ENDF-201 Supplement 1: ENDF/B-V.2 Summary Documentation, to be issued as Brookhaven National Laboratory report BNL-NCS-17541 (1985).

12. E. D. Arthur and P. G. Young, "Evaluated Neutron-Induced Cross Sections for $^{54,56}Fe$ to 40 MeV," Los Alamos National Laboratory report LA-8636-MS (1980) (ENDF-304).

13. E. D. Arthur, P. G. Young, and W. K. Matthes, "Calculations of ^{59}Co Neutron Cross Sections between 3 and 50 MeV," Proc. Symp. on Nuetron Cross Sections from 10 to 50 MeV, Brookhaven National Laboratory report BNL-NCS-51245 (1980), p. 751.

14. O. F. Lemos, "Diffusion Elastique de Particles Alpha de 21 a 29.6 MeV sur des Noyaux de la Region Ti-Zn," Orsay report A 136 (1972).

15. P. Axel, "Electric Dipole Ground State Transition Width Strength Function," Phys. Rev. 126, 671 (1962).

16. J. M. Blatt and V. F. Weisskopf, Theoretical Nuclear Physics (John Wiley and Sons, Inc., New York, 1952).

17. D. W. Muir and E. D. Arthur, "Improved Activation Cross Sections for Vanadium and Titanium," J. Nucl. Materials 122, 1058 (1984).

18. C. Kalbach and F. M. Mann, "Phenomenology of Continuum Angular Distributions I. Systematics and Parameterization," Phys. Rev. C 23, 112 (1981).

19. F. K. McGowan, W. T. Milner, and H. J. Kim, "Nuclear Cross Sections for Charged-Particle Induced Reactions," Oak Ridge National Laboratory report ORNL-CPX-2 (1964).

20. H. Münzel, H. Klew-Nebenius, J. Lange, G. Pfennig, and K. Hemberle, "Karlsruhe Charged-Particle Reaction Data Compilation," Karlsruhe report ISSN-0344-8401 (1979).

21. R. J. Howerton, "ENSL and CDRL: Evaluated Nuclear Structure Libraries," Lawrence Livermore National Laboratory report UCRL-50400, Vol. 23 (1981).

22. C. Michael Lederer and Virginia S. Shirley, Eds., Table of Isotopes, Seventh Edition, John Wiley and Sons (New York), 1978.

23. S. M. Grimes, "Calculation of Spin Cutoff Parameters using Moment Techniques," in Theory and Applications of Moment Methods in Many-Fermion Systems, B. J. Dalton, S. M. Grimes, J. P. Vary, and S. A. Williams, Eds. (Plenum, New York, 1980), p. 273.

24. R. R. Whitehead, "Moment Methods and Lanczos Methods," in Theory and Applications of Moment Methods in Many Fermion Systems, B. J. Dalton, S. M. Grimes, J. P. Vary, and S. A. Williams, Eds. (Plenum, New York, 1980), p. 235.

25. J. P. Jeukenne, A. Lejeune, and C. Mahaux, "Optical-Model Potential in Finite Nuclei from Reid's Hard Core Interaction," Phys. Rev. C 16, 80 (1977).

26. D. Gogny, Nuclear Self-Consistent Fields, G. Ripka and M. Porneuf, Eds. (North-Holland, Amsterdam, 1975).

27. Ch. Lagrange and M. Girod, "Semi-microscopic Calculations of Inelastic Neutron Scattering from Heavy Deformed Nuclei," J. Phys. G: Nucl. Phys. 9, L97 (1983).

28. D. G. Madland and P. G. Young, "Neutron-Nucleus Optical Potential for the Actinide Region," Proc. Int. Conf. on Neutron Phys. and Nucl. Data for Reactors and Other Applied Purposes, Harwell, UK, Sept. 1978, published by OECD, 1978, p. 349.

29. J. A. Grundl and C. M. Eisenhauer, "Fission Spectrum Neutrons for Cross-Section Validation and Neutron Flux Transfer," Proc. Conf. on Nuclear Cross Sections and Technology, Washington, D.C., March 3-7, 1975, Vol. I, p. 250, National Bureau of Standards Special Publication 425, Washington, D.C. (1975).

30. J. Grundl and C. Eisenhauer, "Fission Rate Measurements for Materials Neutron Dosimetry in Reactor Environments," Proc. First ASTM-EURATOM Symp. on Reactor Dosimetry, Petten, Holland, September 22-26, 1975, Part I, p. 425, Commission of the European Communities, EUR 5667 e/f (1977).

31. D. G. Madland and J. R. Nix, "New Calculation of Prompt Fission Neutron Spectra and Average Prompt Neutron Multiplicities," Nucl Sci. Eng. 81, 213 (1982).

32. D. G. Madland and J. R. Nix, "Prompt Fission Neutron Spectra and Average Prompt Neutron Multiplicities," Proc. Specialists' Meeting on Yields and Decay Data of Fission Product Nuclides, Brookhaven National Laboratory, Upton, New York, October 24-27, 1983, p. 423, Brookhaven National Laboratory publication BNL-51778 (1984).

33. W. P. Poenitz and T. Tamura, "Investigation of the Prompt-Neutron Spectrum for Spontaneously-Fissioning ^{252}Cf," Proc. Conf. on Nuclear Data for Science and Technology, Antwerp, Belgium, September 6-10, 1982, p. 465, D. Reidel, Dordrecht (1983).

34. S. Amiel, "Delayed Neutrons in Fission - A Review," Proc. Second IAEA Symp. on Physics and Chemistry of Fission, Vienna, Austria, July 18-August 1, 1969, p. 569, International Atomic Energy Agency, Vienna (1969).

35. J. R. Smith, "Status of ^{252}Cf $\bar{\nu}$ and its Impact on Thermal Reactor Parameters," Proc. Symp. Nuclear Data Problems for Thermal Reactor Applications, Brookhaven National Laboratory, 1978, p. 5-1, Electric Power Research Institute report EPRI-NP-1093 (1979).

36. R. R. Spencer, R. Gwin, and R. Ingle, "A Measurement of the Average Number of Prompt Neutrons from Spontaneous Fission of Californium-252," Nucl. Sci. Eng. 80, 603 (1982).

37. H. T. Heaton II, D. M. Gilliam, V. Spiegel, C. Eisenhauer, and J. A. Grundl, "Fission Cross Sections of ^{235}U, ^{238}U, and ^{239}Pu Averaged over the ^{252}Cf Neutron Spectrum," Proc. NEANDC/NEACRP Specialist Meet. on Fast Neutron Cross Sections of U-233, U-235, U-238, and Pu-239, Argonne National Laboratory, June 28-30, 1976, p. 333, Argonne National Laboratory report ANL-76-90 (1976); updated by J. Grundl, D. Gilliam, D. McHarry, C. Eisenhauer, and P. Soran (May 1982).

38. K. Kobayashi, I. Kimura, and W. Mannhart, "Measurement and Covariance Analysis of Californium-252 Spectrum Averaged Cross Sections," J. Nucl. Sci. Tech. 19, 341 (1982).

39. K. Kobayashi, I. Kimura, H. Gotoh, and H. Tominaga, "Measurement of Average Cross Sections for Some Threshold Reactions of Ti, Cr, and Pb in the Californium-252 Spontaneous Fission Neutron Spectrum Field," Annual Reports of the Research Reactor Inst., Kyoto University 17 (July 1984), pp. 15-21.

40. D. L. Smith, J. W. Meadows, and I. Kanno, "Measurement of the $^{51}V(n,p)^{51}Ti$ Reaction Cross Section from Threshold to 9.3 MeV by the Activation Method," Argonne National Laboratory report ANL/NDM-85, Argonne National Laboratory (June 1984).

41. A. H. Wapstra and G. Audi, "The 1983 Atomic Mass Table," Nucl. Phys. A 432, 1 (1985).

42. D. E. Cullen, K. L. Hill, R. J. Howerton, and S. T. Perkins, "ECSIL: A System for Storage, Retrieval, and Display of Experimental Neutron Data," Lawrence Livermore National Laboratory report UCRL-50400 Vol. 1, Rev. 3 (September 1976).

43. S. T. Perkins and D. E. Cullen, "Experimental and Evaluated Nuclear Plus Interference Cross Sections for Light Charged Particles," Lawrence Livermore National Laboratory report UCRL-50400, Vol. 15, Part F (July 1980).

44. D. M. Hetrick, C. Y. Fu, and D. C. Larson, "Calculated Neutron-Induced Cross Sections for ^{63} ^{65}Cu from 1 to 20 MeV and Comparisons with Experiment," Oak Ridge National Laboratory report ORNL/TM-9083 (ENDF-337) (August 1984).

45. T. Nakamura, M. Yoshida, and K. Shin, "Spectral Measurements of Neutrons and Photons from Thick Targets of C, Fe, Cu, and Pb by 52-MeV Protons," Nucl. Instr. and Meth. 151, 493 (1978).

46. T. Nakamura, M. Fujii, and K. Shin, "Neutron Production from Thick Targets of Carbon, Iron, Copper, and Lead by 30- and 52-MeV Protons," Nucl. Sci. Eng. 83, 444 (1983).

47. H. H. Anderson and J. F. Ziegler, Hydrogen Stopping Powers and Ranges in All Elements, Vol. 3 of The Stopping and Ranges of Ions in Matter (Pergamon Press, New York, 1977).

48. C. B. Fulmer and G. Kindred, "Calculated Residual Radiation Levels for Some Elements Used in Cyclotron Structures," Oak Ridge National Laboratory report ORNL-TM-2834 (August 1970).

49. G. R. Keepin, Physics of Nuclear Kinetics (Addison-Wesley Pub. Co., Inc., Reading, Mass., 1965).

50. S. A. Cox, "Delayed Neutron Data-Review and Evaluation," Argonne National Laboratory report ANL/NDM-5 (April 1974).

51. T. R. England, W. B. Wilson, R. E. Schenter, and F. M. Mann, "Aggregate Delayed Neutron Intensities and Spectra Using Augmented ENDF/B-V Precursor Data," Nucl. Sci. Eng. 85, 139 (1983).

52. L. R. Blue and M. Hoffman, "AIREK III, Generalized Program for the Numerical Solution of Space Independent Reactor Kinetics Equations," Atomics International report AMTD 131 (January 1963).

53. N. A. Fragerio, "Conversion of Reactor Neutrons to 15 MeV with LiD," Argonne National Laboratory report ANL 7870 (1971), p. 10.

54. R. T. Perry and W. B. Wilson, "Neutron Production from (γ,n) Reactions and Spontaneous Fission in ThO_2, UO_2, and $(U,PU)O_2$ Fuels, Los Alamos Scientific Laboratory report LA-8869-MS (June 1981).

55. A. K. Val'mer, P. I. Vatset, L. Ya. Kolesnikov, S. G. Tonapetyan, K. K. Chernyavskii, and A. I. Shpetnyi, "Neutron Yield of the Reactions $^{6}Li(t,n)$ and $^{7}Li(t,n)$," Atomnaya Energiya 10, No. 6 (June 1966), pp. 577-586.

56. G. H. Miley, H. Towner, and N. Ivich, "Fusion Cross Sections and Reactivities," University of Illinois report COO-2218-17 (June 17, 1984).

57. M. A. Lone, D. C. Santry, and W. M. Inglis, "MeV Neutron Production from Thermal Neutron Capture in Li and B Compounds," Nuclear Instruments and Methods 174 (1980), pp. 521-529.

58. N. Jarmie and B. C. Diven, "Li(t,n)Be Thick Target Yields," Nucl. Sci. Eng. 17, No. 3 (November 1963).

59. B. G. Whitmore and W. B. Baker, "The Energy Spectrum of Neutrons from a Po-Be Source," Phys. Rev., 78, No. 6 (June 15, 1950).

60. E. D. Arthur and A. Mutschlecner, Comps., "Applied Nuclear Science Research and Development Semiannual Progress Report: October 1, 1983-May 31, 1984," Los Alamos National Laboratory report LA-10288-PR (January 1985), p. 1.

61. R. M. Wu, R. B. Rothrock, K. D. Dobbin, and J. A. Rawlins, "The Large Core Code Evaluation Working Group Benchmark Problem 5, " Hanford Engineering Development Laboratory (Draft issued December 1983; final report is in preparation).

62. R. J. LaBauve, T. R. England, D. C. George, R. E. MacFarlane, and W. B. Wilson, "LMFBR Neutronics Calculations with the Los Alamos Class VI Computers," Trans. Am. Nucl. Soc. 46, 725 (1984).

63. R. J. LaBauve, D. C. George, T. R. England, W. B. Wilson, and R. E. Mac Farlane, "Calculations for LCCEWG-5: The FFTF HPC Experiment," Los Alamos National Laboratory informal document LA-UR-84-1246 (June 1984).

64. R. J. Barrett and R. E. MacFarlane, "The MATXS-TRANSX System and the CLAW-IV Nuclear Data Library," Proc. Int. Conf. Nucl. Cross Sections for Tech., October 22-26, 1979, Knoxville, Tenn. (NBS Special Publication 594, 1980), p. 213.

65. K. L. Derstine, "DIF3D: A Code to Solve One-, Two-, and Three-Dimensional Finite-Difference Diffusion Theory Problems," Argonne National Laboratory report ANL-82-64 (April 1984).

66. W. B. Wilson, T. R. England, R. J. LaBauve, and R. E. Schenter, "CINDER-3-Depletion Code for Class VI Computers," Trans. Am. Nucl. Soc. 46, 726 (1984).

67. R. Kinsey, Comp., "ENDF-201: ENDF/B Summary Documentation," Brookhaven National Laboratory report BNL-NCS-17541 (ENDF-201), 3rd Ed. (ENDF/B-V) (1979).

68. R. E. MacFarlane, D. W. Muir, and R. M. Boicourt, "The NJOY Nuclear Data Processing System, Volume I: User's Manual," Los Alamos National Laboratory report LA-9303-M (ENDF-324) (May 1982).

69. W. F. Walters, F. W. Brinkley, and D. R. Marr, "User's Guide for TWOHEX: A Code Package for Two-Dimensional, Neutral-Particle Transport in Equilateral Triangular Meshes," Los Alamos National Laboratory report LA-10258-M Manual (October 1984).

70. R. D. O'Dell, "Standard Interface Files and Procedures for Reactor Physics Codes, Version II," Los Alamos National Laboratory report LA-6941-MS (September 1977).

☆ U.S. GOVERNMENT PRINTING OFFICE 1985—676-034/20141

Printed in the United States of America
Available from
National Technical Information Service
US Department of Commerce
5285 Port Royal Road
Springfield, VA 22161

Microfiche (A01)

Page Range	NTIS Price Code	Page Range	NTIS Price Code	Page Range	NTIS Price Code	Page Range	NTIS Price Code
001-025	A02	151-175	A08	301-325	A14	451-475	
026-050	A03	176-200	A09	326-350	A15	476-500	
051-075	A04	201-225	A10	351-375	A16	501-525	
076-100	A05	226-250	A11	376-400	A17	526-550	
101-125	A06	251-275	A12	401-425	A18	551-575	
126-150	A07	276-300	A13	426-450	A19	576-600	
						601-up*	

*Contact NTIS for a price quote.

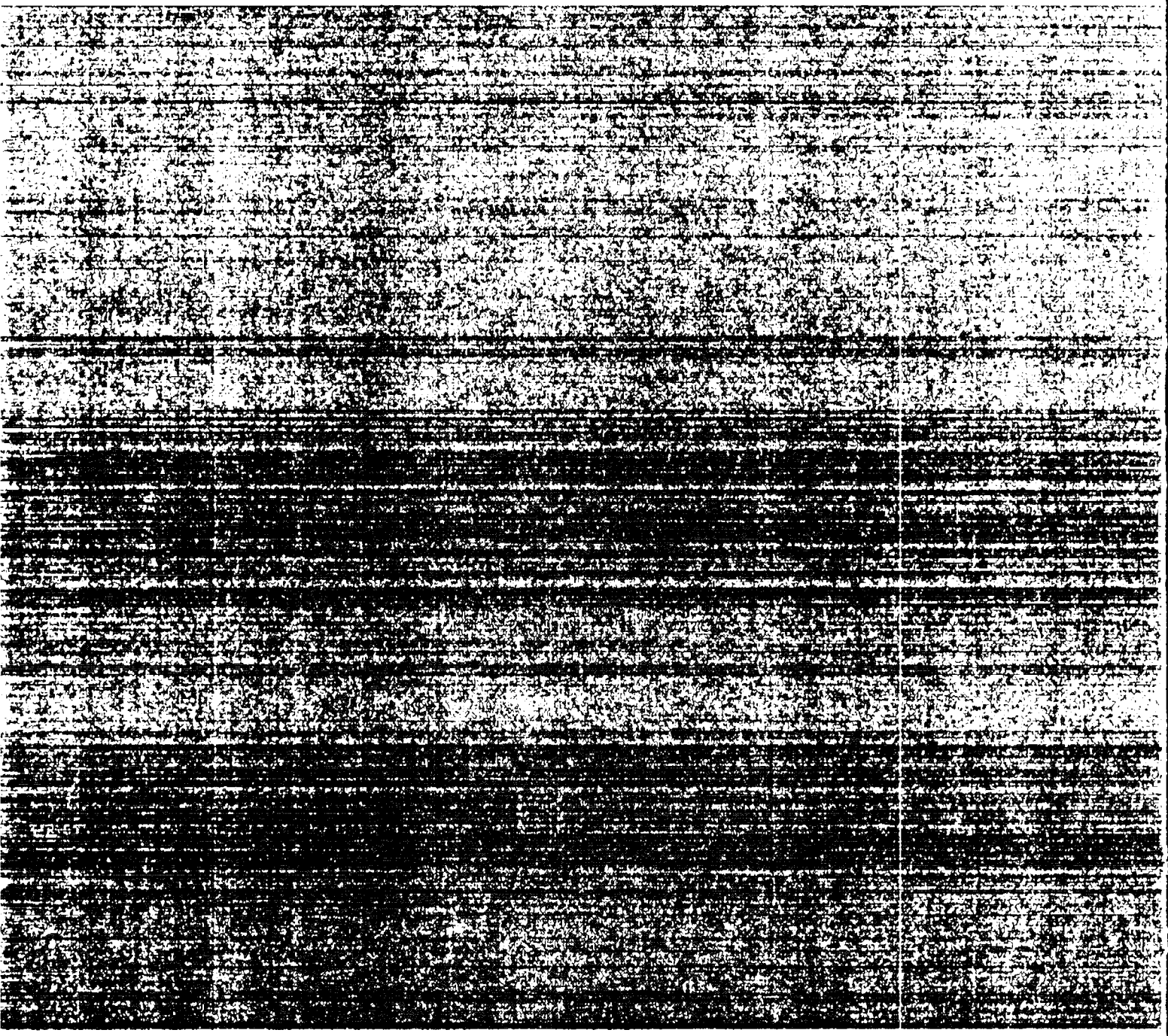

Los Alamos